



**Environmental
Science**
Nano

Environmental routes of virus transmission and the application of nanomaterial-based sensors for virus detection

Journal:	<i>Environmental Science: Nano</i>
Manuscript ID	EN-CRV-06-2022-000600.R1
Article Type:	Critical Review

SCHOLARONE™
Manuscripts



Double-Anonymised Title Page

Authors:

Wei Wang,^{1ab} Seju Kang,^{1ab} Wei Zhou,^c and Peter J. Vikesland^{*ab}

¹ These authors contribute equally to the work

Affiliations:

a Department of Civil and Environmental Engineering, Virginia Tech, Blacksburg, Virginia 24061, United States

b Virginia Tech Institute of Critical Technology and Applied Science (ICTAS) Sustainable Nanotechnology Center (VTSuN), Blacksburg, Virginia 24061, United States

c Department of Electrical and Computer Engineering, Virginia Tech, Blacksburg, Virginia 24061, United States

Acknowledgements:

This research was supported by the US National Science Foundation grants OISE-1545756 and CBET-2029911. Additional support was provided by the Sustainable Nanotechnology Interdisciplinary Graduate Program (VTSuN IGEP) funded by the Virginia Tech Graduate School. We thank Dr. Linsey C Marr at Virginia Tech for valuable comments on the virus transmission in the environment.

Author contributions:

W. Wang and S. Kang directed the research effort, did the literature review, wrote the manuscript, and provided oversight of the research team. W. Zhou aided in the writing of the manuscript. P.J. Vikesland obtained the research funding, provided oversight of the project, and collaborated in the writing and editing of the manuscript. All authors contributed to the development of the manuscript and its revision.

Environmental routes of virus transmission and the application of nanomaterial-based sensors for virus detection

Abstract

Many outbreaks of emerging disease (e.g., avian influenza, SARS, MERS, Ebola, COVID-19) are caused by viruses. In addition to direct person-to-person transfer, the movement of these viruses through environmental matrices (water, air, and food) can further disease transmission. There is a pressing need for rapid and sensitive virus detection in environmental matrices. Nanomaterial-based sensors (nanosensors), which take advantage of the unique optical, electrical, or magnetic properties of nanomaterials, exhibit significant potential for environmental virus detection. Interactions between viruses and nanomaterials (or recognition agents on the nanomaterials) can induce detectable signals and provide rapid response times, high sensitivity, and high specificity. Facile and field-deployable operations can be envisioned due to the small size of the sensing elements. In this frontier review, we summarize virus transmission via environmental pathways and then comprehensively discuss recent applications of nanosensors to detect various viruses. This review provides guidelines for virus detection in the environment through the use of nanosensors as a tool to decrease environmental transmission of current and emerging diseases.

Keywords: virus, transmission, detection, nanomaterial, sensor

Environmental significance

Numerous viruses (including SARS-CoV-2) can spread across various environmental matrices (e.g., air, soil, water, and food), promoting direct/indirect infection transmission. Environmental monitoring of viruses is highly desirable to prevent the spread of infectious diseases. Nanomaterial-based sensors (nanosensors) have recently shown great potential for virus detection with low-cost, high sensitivity, and short analysis time. The small size and the adaptability of nanosensors enable field-deployable virus detection in various environmental matrices. This review provides guidelines for nanosensor application for virus detection to control the environmental transmission of current and emerging diseases associated with viruses.

1. Introduction

Respiratory viruses can spread from person to person and cause contagious respiratory illnesses. Outbreaks of viral disease have regularly occurred and have caused hundreds of thousands of fatalities over the last three decades: severe acute respiratory syndrome coronavirus (SARS-CoV) in 2003,¹ influenza A virus H1N1 subtype in 2009,² Ebola virus (EBOV) in 2014,³ middle east respiratory syndrome coronavirus (MERS-CoV) in 2014,⁴ and Zika virus (ZIKV) in 2014.⁵ Currently, the ongoing COVID-19 (caused by the SARS-CoV-2 virus) pandemic is the world's most pressing public health threat and as of June 2022 has resulted in known infections in greater than 529 million people across the world.⁶ To minimize morbidity and mortality, rapid virus detection and contact tracing along routes of virus transmission are crucial.⁷ In addition to direct transfer between infectious and susceptible individuals, viruses can also be transmitted through environmental media such as water, air, and food.⁸ For instance, SARS-CoV-2 spreads not only through person-to-person contact, but also via contaminated fomites and respiratory aerosols.⁹ The survival and transport of viruses within and across environmental matrices promotes indirect transmission.¹⁰ Detection of viruses in these environmental matrices is required to fully track all routes of virus transmission, determine undiagnosed infections at the population/community level,¹¹ and control the spread of disease.

Current virus detection methods include plaque assays, polymerase chain reaction (PCR) based techniques, loop-mediated isothermal amplification (LAMP), and enzyme-linked immunosorbent assay (ELISA). The standardized operation procedures and high sensitivity of these methods render them widely applicable, but primarily located in clinical or laboratory settings. Tedious pretreatment steps and huge investments in chemicals or instruments often hamper their application for environmental samples, especially for the large number of samples

1
2
3 required to track viral transmission routes. There is an urgent need for lower-cost, field deployable
4 devices, as well as high sensitivity and specificity that consider environmental diagnostic
5 applications.
6
7
8
9

10 Nanomaterial-based sensors (nanosensors) have shown significant promise towards virus
11 detection in the environment due to their small size, low-cost, high sensitivity, and rapid
12 turnaround time. **Error! Reference source not found.** summarizes the principal components of a
13 nanosensor. The basic principle is to transform stimuli arising from the interaction between a given
14 nanomaterial and a target analyte of interest into a quantifiable signal, termed signal transduction.
15 Nanosensors employ a range of signal transduction mechanisms enabled by functionalizing
16 nanomaterials with different recognition elements such as aptamers, peptides, and antibodies¹²,
17 that render high specificity. Three types of signal transduction have been broadly applied in
18 nanosensors: optical, electrical, and magnetic.¹³ Such signal transduction enables higher sensitivity
19 and stability over traditional methods. Nanomaterials have several advantages over bulk materials.
20 Nanomaterials have completely different physiochemical properties (e.g., durability, conductivity,
21 and quantum effects at nanoscale) from those of bulk materials. Also, they have high surface-to-
22 volume ratio which help close contact with surrounding macromolecules (e.g., DNA, virus,
23 protein), thus affecting reactivity. Different nanoparticle morphologies and properties can be
24 harnessed for nanosensor development. Plasmonic nanomaterials such as gold and silver
25 nanoparticles (AuNPs, AgNPs) or photoconductive materials (e.g., carbon nanotubes (CNTs))
26 have been used to develop optical nanosensors. For the development of electrical nanosensors,
27 both one-dimensional nanomaterials (e.g., silicon nanowires (SiNWs), CNTs) and two-
28 dimensional nanomaterials (e.g., graphene/graphene oxide (GO) and metal-organic frameworks
29 (MOFs) nanosheets) have been used. Lastly, iron-based nanoparticles (e.g., Fe⁰, Fe₃O₄, γ-Fe₂O₃)
30
31
32
33
34
35
36
37
38
39
40
41
42
43
44
45
46
47
48
49
50
51
52
53
54
55
56
57
58
59
60

are commonly used to develop magnetic nanosensors. Such nanomaterials can be incorporated within flexible substrates such as paper or lateral flow-devices to be low-cost and field-deployable and are thus suitable for environmental applications. Despite that, the application of nanosensors for virus detection in the environment still has not been heavily explored. In this review, we emphasize the necessity of virus detection in environmental matrices by introducing environmental viral transmission routes and then review the latest progress toward the developments of nanosensors for virus detection to discuss the feasibility and potential challenges for their application for environmental sample interrogation.

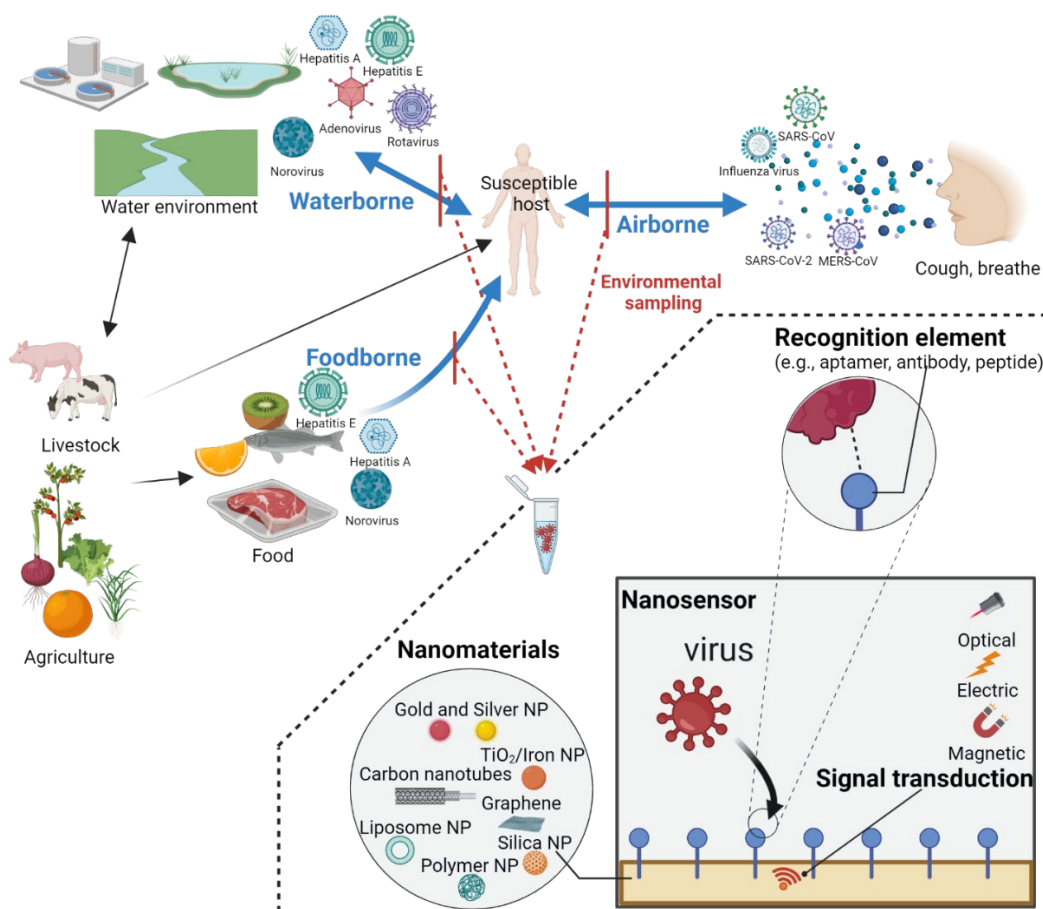


Figure 1. Schematic diagram of three major virus transmission pathways (i.e., waterborne, airborne, and foodborne) to a susceptible host and the application of nanosensors for virus detection. Environmental sampling is followed by nanosensor-enabled detection of viruses. The principal components of a nanosensor for virus detection include signal transduction, recognition element, and nanomaterials.

2. Virus transmission routes in the environment

Viruses can spread in the environment and infect people through inhalation and ingestion. Water, air, and food are key environmental media known to play a role in virus transmission (**Figure 1**).¹⁴ For example, viruses can be discharged into sewage along with the feces of infected people or animals and can spread when water circulates or when transmitted into the air.¹⁵ Droplets and aerosol particles produced when infected patients cough, sneeze, speak, and breathe are important carriers for the environmental distribution of viruses.¹⁶ Viruses may also spread disease through the food chain or contact between infected individuals and prepared foods. Detection of viruses in these different environments is required to track the routes of virus transmission.

2.1 Waterborne transmission

Waterborne viruses such as hepatitis A and E virus (HAV and HEV), norovirus (NoV), adenovirus (AdV), and rotavirus (RV) are enterally transmitted and are primary causes of waterborne disease.¹⁷ One obvious route of waterborne virus transmission is the discharge of sewage and sewage-contaminated waters into drinking water sources. Wastewater is considered one of the most concentrated environmental virus reservoirs with an estimated mean concentration of 7000 infectious enteric viruses per liter since viruses are discharged into sewage along with the feces and urine of infected people or animals.¹⁸ High titers of the infectious virus have been measured in wastewater samples collected worldwide.^{19, 20} For example, SARS-CoV-2 RNA has been detected in wastewater and can be used as a potential early warning system for COVID-19 transmission in the community.²¹⁻²³ Although some wastewater treatment processes may remove viruses, their removal efficiency is often limited. One report suggests that primary treatment achieves only $\sim 1 \log_{10}$ removal of NoV.²⁴ The same study found that activated sludge was more

1
2
3 effective for NoV removal (2.3-3.1 log₁₀) than trickling filters, biological aerated filters, and
4 humus tanks. Further, UV disinfection of the final effluent only led to 0.8-1 log₁₀ NoV reduction.
5
6 Hence, viable viruses can be released into environmental waters via the discharge of treated
7 effluent. Pang et al. investigated the occurrence of viruses in six major rivers in Alberta by
8 quantitative PCR (qPCR) after concentrating samples by the adsorption-elution method and found
9 that RV was the most prevalent virus (concentrations ranging from 2.3 to 4.5 log₁₀ genomic
10 equivalent copies/L) and had a seasonal peak during winter.²⁵ NoV, sapovirus, astrovirus, AdV,
11 and John Cunningham virus also peaked during the winter. Some viruses are environmentally
12 resilient and may be transmitted through surface water, groundwater, and drinking water resources.
13
14 Lee et al. investigated the occurrence of NoV in 71 sampling sites in South Korea by reverse
15 transcription (RT)-PCR after concentrating samples by the adsorption-elution technique, and
16 found that 48.3% (summer) and 35.3% (fall-winter) of the samples were positive.²⁶ Miura et al.
17 collected river water samples at 21 drinking water treatment plants in Japan from June 2017 to
18 August 2018 by RT-PCR after concentrating sample by adsorption-elution technique and found
19 that the detection rate for NoV GII (gene type) and RV (group A) were 87% and 100%,
20 respectively.²⁷ Fortunately, the total number of viral reads at the point of use (e.g., tap water) was
21 ~0.1% of that in raw river water except for HEV where it was 2.2%.²⁸ Although the risk of getting
22 infected by viruses in tap water is expected to be relatively low due to their concentrations, there
23 remains a possibility of transmission to other environments during outbreaks. In addition, evidence
24 indicates the presence of viable viruses in aquatic matrices such as seawater and reuse water.^{29, 30}

2.2 Airborne transmission

51 Airborne viruses are transmitted by aerosolized droplets or particles produced when
52 infected individuals cough, sneeze, speak, and breathe.^{16, 31} Droplets and aerosol particles
53
54
55
56
57
58
59
60

1
2
3 produced by these respiratory activities span a wide range of sizes, and some can remain suspended
4
5 in the air for seconds to hours, can travel long distances, and can accumulate in poorly ventilated
6
7 spaces.³² Aerosol-based dissemination can lead to the widespread transmission of viruses.
8
9 Influenza, measles, and coronavirus (SARS-CoV or SARS-CoV-2) are well-known airborne
10
11 viruses.^{16, 33-35}
12
13

14
15 Airborne virus concentrations are highest in indoor environments characterized by poor
16
17 ventilation, large numbers of people, confined space, and the presence of viral sources. For
18
19 example, a hospital is where viruses can quite readily spread through the air from infected
20
21 individuals. Researchers have found that influenza viral RNA could be detected in fever clinics
22
23 for confirmed flu patients and visitors although there were no viruses in the outpatient hall and
24
25 clinical laboratory.³⁶ Similarly, SARS-CoV-2 RNA was detected with a concentration of several
26
27 gene copies per cubic meters in aerosols from patient toilet areas in Fangcang Field Hospital in
28
29 Wuhan by collecting aerosol samples on a filter, extracting RNA in dissolved solution and
30
31 analyzing by PCR.³⁷ The concentrations of airborne viruses in most places within hospitals
32
33 (isolation wards and ventilated patient rooms) are usually low thus suggesting that room ventilation
34
35 and open spaces can effectively reduce viral loads. Schools and offices are crowded public places
36
37 at high-risk of airborne virus transmission, especially during the flu season. Xie et al. investigated
38
39 the occurrence of several airborne viruses in air samples collected by bioaerosol samplers in a
40
41 university campus by RT-PCR and found that influenza A and B viruses were detectable at higher
42
43 frequencies than other viruses (rhinovirus, respiratory syncytial virus, and human coronavirus).³⁸
44
45 The school corridor had the highest influenza A virus concentration relative to classrooms and
46
47 gyms in an elementary school due to the high passing frequency and air turbulence caused by
48
49 students' activities.³⁹ In contrast, the influenza A virus was not detected in any tested outdoor
50
51
52
53
54
55
56
57
58
59
60

1
2
3 samples. Besides the physical spaces, the indoor environment conditions such as temperature and
4 relative humidity (RH) have been identified as important factors in airborne virus survival and
5 transmission.^{40, 41} Cold temperatures and low RH favor the spreading of airborne viruses due to
6 their positive effects on virus stability.⁴²
7
8
9
10
11

12 **2.3 Foodborne transmission**

13
14 Foodborne viruses are a significant cause of human morbidity and mortality. Fresh food
15 can be contaminated at any step between preharvest and postharvest.⁴³ Foodborne viral infections
16 are often transmitted via the fecal-oral route through ingesting contaminated food and illness
17 across the food chain.⁴⁴ HAV and NoV are recognized as two of the most important foodborne
18 viruses^{43, 45} and are regularly detected in shellfish, fresh fruits, and vegetables. SARS-CoV-2 is
19 also detected from frozen cod packaging.⁴⁶
20
21
22
23
24
25
26
27

28 Using contaminated irrigation water and agricultural soils is a primary route of viral
29 transmission during preharvest. The transfer of viruses from irrigation water to plants can occur
30 through direct contact or internalization into plant tissue via the root system.⁴⁴ In field experiments,
31 Brassard et al. found that although the concentration of viruses in irrigation water was extremely
32 low, NoV and swine HEV could be detected in strawberry samples after being irrigated with
33 contaminated water for several days.⁴⁷ These results indicate that fruits might concentrate the
34 viruses during the growth to pose a threat to human beings. Similar results were found in some
35 fresh fruit and vegetables and their associated agricultural and environmental samples in South
36 Korea.⁴⁸ These results suggest that removing viruses from irrigation water may successfully
37 minimize the transmission of foodborne viruses during preharvest.
38
39
40
41
42
43
44
45
46
47
48
49
50

51 During harvest and postharvest, foodborne viruses can be traced to foods handled by
52 infected food handlers (e.g., field harvesters, production plant workers, professional chefs).
53
54
55
56
57
58
59
60

1
2
3 Shellfish, fruits, and vegetables are at high risk for transmitting viruses since they undergo
4 extensive human handling during production. To check whether the infected food handlers will
5 cause secondary contamination in food samples, Somura et al. recovered NoV in food samples
6 using bacterial culture method in Tokyo from five NoV outbreaks during 2015-2016. It was found
7 that each partial NoV *VPI* sequence of NoV-positive food samples matched completely with those
8 in NoV-positive individuals and food handlers, which proved food handlers played a potentially
9 important role in NoV transmission.⁴⁹ Similar results have been obtained by other researchers that
10 food handling practices carry potential risk of acute gastroenteritis outbreaks.⁵⁰ Besides, recent
11 research has shown that SARS-CoV-2 can remain highly stable on frozen food and that
12 contaminated cold-storage foods may pose a risk for SARS-CoV-2 transmission between countries
13 and regions.⁵¹ These results indicate that the development of safe food-handling strategies among
14 food handlers is important in controlling the transmission of foodborne viruses.

30 **2.4 Current virus detection approaches**

31
32
33 Before discussing nanosensor applications for virus detection, we briefly summarize
34 current approaches to virus detection. The standard method to detect the pathogenic virus is the
35 plaque assay. The plaque assay counts the number of plaque-forming units (PFU) in a certain
36 volume of liquid. In this assay, various virus dilutions are incubated in the presence of a monolayer
37 of recipient host cells. A viral plaque forms when the virus infects the recipient cells. The viral
38 concentration is then determined using either PFU or the 50% tissue culture infectious dose
39 (TCID₅₀). The plaque assay has several limitations, such as the required long incubation period for
40 plaque formation, laborious counting effort, and the limited availability of recipient host cells for
41 many viruses of health concern.⁵²

1
2
3 Nucleic acid amplification strategies such as PCR and LAMP have been widely used to
4 detect viruses.^{53, 54} PCR and LAMP approaches require the extraction of DNA or RNA from a
5 virus. Following this step, enzyme-linked gene amplification enables the detection of target genes.
6
7 For RNA detection, extracted RNA needs to be reverse-transcribed to complementary DNA using
8 a reverse transcriptase enzyme prior to amplification. PCR generally relies upon *Taq* polymerase
9 to replicate the target gene over multiple thermal cycles. For this process, two primers are designed
10 to target the amplified gene region. In contrast, LAMP relies upon four different primers that bind
11 to six distinct regions of target DNA. *Bst* polymerase is used to displace strands at a constant
12 temperature and replicate the target gene. LAMP has greater specificity and a shorter turnaround
13 time (~0.5 to 1 hour) than PCR. Further, PCR approaches require skilled personnel and high-cost
14 facilities.⁵⁵ Such an entry barrier limits the proactive detection of infectious viruses. While LAMP
15 is gaining attention as a PCR alternative owing to its fast turnaround time and field deployability,
16 the high rate of false positives makes the development of LAMP-based assays challenging.⁵⁶⁻⁵⁸
17 RT-PCR and RT-LAMP assays for detection of SARS-CoV-2 have LODs of 484 and 200
18 copies/mL.^{59, 60}

19
20
21
22
23
24
25
26
27
28
29
30
31
32
33
34
35
36
37
38 ELISA can detect viruses using selective complexation between an antigen and an antibody
39 linked to an enzyme. A specific antibody conjugated substrate is used to capture the target virus,
40 followed by an enzyme attachment. Commonly, horseradish peroxidase (HRP)-conjugated goat
41 anti-mouse immunoglobulin (IgG) is used as the enzyme. HRP catalyzes the oxidation of 3',5,5'-
42 tetramethylbenzidine (TMB) by hydrogen peroxide (H₂O₂) and the optical signal arising from the
43 production of oxidized TMB enables virus detection. ELISA assay for detection of SARS-CoV-2
44 IgG has a LOD of 0.0736 µg/mL.⁶¹ Despite its success in virus detection, ELISA suffers from
45 laborious assay procedures and poor sensitivity under real-world application conditions.⁶²
46
47
48
49
50
51
52
53
54
55
56
57
58
59
60

3. Applications of nanosensors for virus detection

Due to the unique optical, electrical, or magnetic properties, nanosensors have shown significant potential for virus detection. This section comprehensively discusses recent nanosensor applications for virus detection. We summarize the discussed nanosensors in **Table 1** for SARS-CoV-2, **Table 2** for influenza virus due to their focus in recent times and the massive reference databases, and **Table 3** for other viral targets. In each table, we conclude the main recognition elements, sensing strategy and the limit of detection (LOD) of each sensor. LOD is one of the most important criteria to be considered for environmental application, especially for tracking virus transmission in which viral concentration may go down to zero if the distance away from a source is far. We emphasize that the LODs and units listed in the tables reflect those reported in the original work. While conversion of these units into a standardized set of reporting units would be ideal, it was considered outside the scope of the present work due to the many assumptions required for such calculations.

3.1 Optical nanosensors

Nobel metal (e.g., Au or Ag) NPs can support localized surface plasmon resonance (LSPR) modes,^{63, 64} the collective oscillation of conductive band electrons in metal NPs by free-space light excitation, to concentrate intense optical fields at the nanoscale.⁶⁵ Therefore, such plasmonic nanomaterials have been used as highly sensitive optical nanosensors across the fields of analytics, food safety, biomedicine, and environmental science.⁶⁶⁻⁷⁰ Fluorescent nanomaterials, such as semiconductor quantum dots (QDs)^{71, 72} and lanthanide-doped NPs⁷³, can serve as down-conversion and up-conversion fluorescence emission nanoprobe for fluorometric sensing approaches.

1
2
3 To date, several virus sensing approaches have been developed that rely upon optical
4 nanomaterials. Because of the large volume of literature on optical nanosensors, herein we exclude
5 works on the detection of viral nucleic acid that precedes gene amplification (e.g., plasmonic NP-
6 based-colorimetric method coupled with PCR for detection of SARS-CoV-2 RNA⁷⁴). More
7 detailed reviews on viral nucleic acid detection using optical nanosensors can be found in the
8 recent literature.^{75, 76} The following section splits into three parts according to the optical signal
9 readout device: colorimetric, surface-enhanced Raman scattering (SERS), and fluorometric.

10 11 12 13 14 15 16 17 18 19 20 **3.1.1 Colorimetric nanosensors**

21
22 Colloidal noble metal NPs can be uniformly dispersed in suspension. The color of noble
23 metal NPs reflects the LSPR resonant absorption and scattering properties depending on their sizes,
24 shapes, and the surrounding local environment.⁷⁷ Notably, Au and Ag NPs of the same shape and
25 size can exhibit different colors in the visible to near-infrared (NIR) region due to the additional
26 interband-transition induced optical absorption in AuNPs. Colorimetric sensing approaches
27 generally rely upon color changes that can be measured by a UV-Vis spectrophotometer or
28 identified by the naked eye. Aggregation of noble metal NPs through conjugation with a target
29 virus results in an absorbance peak shift (i.e., red-shift). Recently, AuNPs functionalized with
30 antibodies targeting three SARS-CoV-2 proteins (spike, envelope, membrane) were achieved by
31 colorimetric detection.⁷⁸ The absorbance peak (560 nm) of a colloidal suspension of AuNPs
32 exhibited a red-shift a few minutes after mixed with a SARS-CoV-2-containing sample. Often,
33 colloidal plasmonic NPs exhibit non-specific binding in resource-constrained settings due to the
34 high susceptibility of the approach to perturbations in their external environment.⁷⁹ To overcome
35 this challenge, Xiong et al. induced the disassembly of gold nano-aggregates through contact with
36 enterovirus 71 (EV71).⁸⁰ Specifically, negatively charged AuNPs dispersed in solution were
37
38
39
40
41
42
43
44
45
46
47
48
49
50
51
52
53
54
55
56
57
58
59
60

1
2
3 aggregated due to the addition of positively charged peptides, resulting in a blue-colored
4 suspension. In the presence of EV71, the target antibody immunoassay system releases a liposome
5 encapsulating multiple enzymes that hydrolyze the positively charged peptide, thus promoting the
6 disassembly of AuNP aggregates. This approach successfully allows EV71 detection with a LOD
7 of 16 copies/ μ L.
8
9

10
11
12
13
14
15 In place of using an aggregation strategy, AuNPs can also be coupled with an Ag staining
16 technique for colorimetric virus detection. In this approach, silver ions in proximity to an AuNP
17 surface are reduced by a reducing agent. The AuNPs transfer an electron from the reducing agent
18 to a silver ion and catalyze formation of a silver metal film on the AuNP surface. The continuous
19 deposition of silver layer over Au by this process produces a gray color and the intensity of
20 developed color can be monitored. Recently, this technique was applied within a microfluidic
21 device for multiplex virus detection.⁸¹ In this study, the authors used the systematic evolution of
22 ligands by exponential enrichment (SELEX) to generate aptamer recognition elements that have
23 an affinity for ZIKV and chikungunya virus (CHIKV) envelope proteins. In the presence of those
24 proteins, the aptamer functionalized microfluidic device forms a sandwich structure with AuNPs
25 conjugated with the same aptamer. Following sandwich formation, silver reagents were introduced
26 onto the surface of AuNPs, and the silver layer was formed. The intensity of the digitized gray
27 color as measured by ImageJ (CMYK model) showed a linear correlation with the concentration
28 of virus proteins and LODs of 1 pM in phosphate-buffered saline (PBS) and 100 pM in calf blood.
29
30
31
32
33
34
35
36
37
38
39
40
41
42
43
44
45
46

47 The coupling of plasmonic and magnetic NPs has also been applied in colorimetric assays.
48 It was reported that an aptamer conjugated maghemite (γ -Fe₂O₃) and AuNP hybrid nanocomposite
49 enabled rapid visual detection of dengue virus (DENV).⁸² For sensitive detection of influenza A
50 virus H1N1, a magnetic nanozyme-linked immunosorbent assay (MagLISA) was developed
51
52
53
54
55
56
57
58
59
60

1
2
3 **(Figure 2).**⁸³ The enzyme-like activity of AuNPs known as Au nanozymes (AuNZs) catalyzed
4 oxidation of TMB (colorless) by H₂O₂. When TMB is oxidized it produces a blue color. Antibody
5 conjugated Fe₃O₄ and AuNPs form a sandwich complex in the presence of H1N1. This complex
6
7 can be separated via applying a magnetic field and then re-suspended in colorizing agent-
8 containing solution (H₂O₂ and TMB). The color change is then monitored at 450 nm, showing
9
10 positive linearity with the H1N1 concentration and a LOD of 4.42×10⁻¹⁴ g/mL. Clinically isolated
11
12 influenza A virus H3N2 from patients could be successfully separated from human serum by this
13
14 platform and detected with a LOD of 2.5 PFU/mL. Additionally, other peroxidase-like AuNP-
15
16 based substrates have been applied for colorimetric virus detection. To improve their catalytic
17
18 activity, AuNPs can be coupled with CNTs and graphene. For instance, an antibody-conjugated
19
20 AuNP-CNT hybrid substrate was applied for influenza A virus H3N2 detection.⁸⁴ H3N2 was
21
22 attached to the bottom of a polystyrene 96-well followed by the addition of antibody-conjugated
23
24 AuNP-CNTs. After several wash cycles to remove non-deposited AuNP-CNTs, a mixture of TMB
25
26 and H₂O₂ was added. More AuNP-CNTs were attracted in higher concentration virus solutions,
27
28 which showed higher catalytic activity. In this case, more TMB could be oxidized, resulting in the
29
30 development of a detectable blue color. This method showed a LOD of 3.4 PFU/mL. The same
31
32 procedure was conducted using an AuNP-graphene hybrid substrate to detect NoV-like NPs (NoV-
33
34 LPs).⁸⁵ The LOD of the method was 92.7 pg/mL.

35
36
37
38
39
40
41
42
43
44
45 In place of AuNP-based substrates, vanadium oxide (V₂O₅) NPs have also been applied
46
47 for peroxidase-like catalytic activity-based colorimetric virus sensing.⁸⁶ V₂O₅ NPs have the great
48
49 catalytic ability and robust stability. V₂O₅-encapsulated liposomes (VONP-LPs) and Fe₃O₄ NPs
50
51 were conjugated with an antibody specific to NoV-LPs. After complexation of VONP-LPs, Fe₃O₄
52
53 NPs, and NoV-LPs via antigen-antibody interactions, the magnetically separated sample was
54
55
56
57
58
59
60

1
2
3 subjected to Triton X induced liposome hydrolysis. The release of V_2O_5 NPs catalyzes the
4 oxidation of TMB by H_2O_2 and produces an intense blue color. The V_2O_5 NPs also enhance the
5 redox signal in the differential pulse voltammetry (DPV) spectrum, thus enabling electrochemical
6 sensing. Linear trends between the concentrations of NoV-LPs and the corresponding optical and
7 electrochemical signals in different ranges were confirmed. The dual-modality sensor showed
8 LODs of 0.34 pg/mL and 4.1 fg/mL for optical and electrochemical sensing approaches,
9 respectively.
10
11
12
13
14
15
16
17
18

19 The formation of spherical polydiacetylene (PDA) vesicles through the self-assembly of
20 monomer PDAs can be used for optical virus sensing. Unperturbed PDA vesicles exhibit an intense
21 blue color due to electronic absorption by the conjugated backbone. Virus attachment to PDA
22 vesicles induces backbone distortion, thus resulting in a blue-to-red color change. Using a peptide-
23 functionalized PDA nanosensor for recognizing influenza A virus H1N1, sensitive colorimetric
24 detection was achieved.⁸⁷ This peptide has a high affinity against H1N1 viruses compared with
25 others (H3N2, H5N2, and H6N5). When a peptide on a PDA vesicle contacted with the virus,
26 absorbance at 550 (red) and 628 (blue) nm were measured, and the colorimetric responses were
27 calculated based on these changes. The results demonstrated the applicability of the peptide-
28 functionalized PDA nanosensor for the detection of H1N1 with a LOD of 10^5 PFU. In place of the
29 peptide, the antibody conjugated PDA nanosensor has also been coupled with the polyvinylidene
30 difluoride membrane for paper-based virus detection.⁸⁸
31
32
33
34
35
36
37
38
39
40
41
42
43
44
45
46

47 In addition to detectable color changes, the absorbance shift of plasmonic nanostructures
48 in the presence of virus can also be recorded by LSPR sensors. Detection sensitivity based upon
49 LSPR shift measurements is dependent on the design and the fabrication of plasmonic
50 nanostructures. An ordered array of triangular Au nanopillars was fabricated for the development
51
52
53
54
55
56
57
58
59
60

1
2
3 of the LSPR sensor based on an octupolar geometry with a minimum interparticle distance between
4 two-unit cells of 25 nm.⁸⁹ This interparticle distance produces a non-negligible coupled field
5
6 between the unit cells and the nanostructure exhibits an absorbance peak in the near-infrared region
7
8 at 735 nm that undergoes a red-shift when analytes attach and increase the local refractive index.
9
10 The group found the bulk refractive index sensitivity of the substrate, 280 nm/refractive index unit,
11
12 was greater than for any previous substrate. The substrate was functionalized with antibody 2B4
13
14 for the detection of RV. The optimal antibody concentration (25 µg/mL) on Au surface attachment
15
16 was confirmed to obtain a proper configuration with no rotation or deformation and a
17
18 corresponding higher efficiency for virus trapping. With excess antibody attachment, the access of
19
20 viruses to the substrate can be sterically inhibited. The LOD of this LSPR nanosensor was
21
22 estimated to 126 PFU/mL.
23
24
25
26
27

28 Overall, colorimetric virus detection methods show great sensitivity. Additionally, color
29
30 changes from virus contact to sensing platforms can be detectable by the naked eye or by cell-
31
32 phone camera-based methods,⁹⁰ enabling straightforward detection without the need for dedicated
33
34 read-out devices. Hence, we anticipate that research focusing on the simple design of colorimetric
35
36 assays will be highly advantageous. Furthermore, the insufficient colloidal stability of many
37
38 colloidal NPs has been found in real samples characterized by macromolecules, natural organic
39
40 matter, and high ionic can interfere with detection.^{79, 91} Stabilizing agents that can resist such
41
42 interferents should be developed and the applicability of the probes in real environmental samples
43
44 must be explored.
45
46
47
48
49
50
51
52
53
54
55
56
57
58
59
60

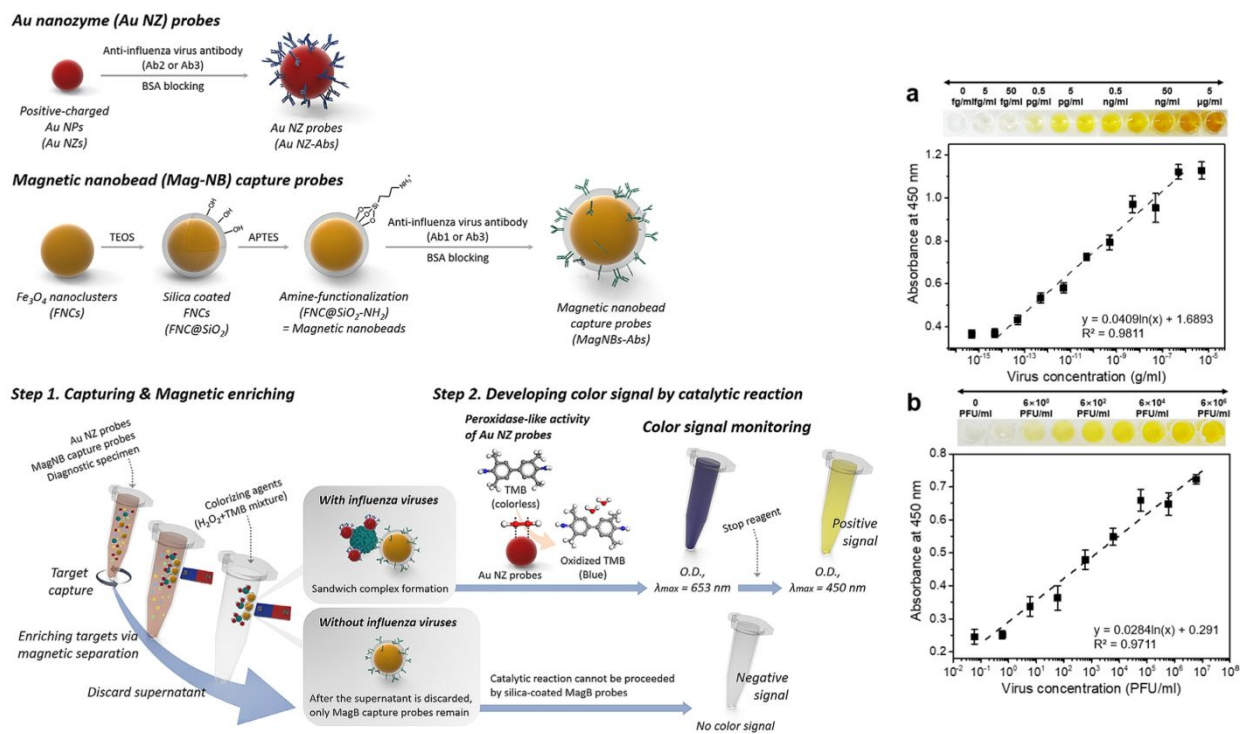


Figure 2. Colorimetric detection of the virus. Au nanozyme (AuNZ) and magnetic nanoprobe (Mag-NB) were synthesized and functionalized with antibodies to capture the virus and enrich them using a magnetic field. A magnetic nanozyme-linked immunosorbent assay (MagLISA) uses antibody conjugated AuNZs and Mag-NBs to capture the virus and enrich them using a magnetic field. The complexation of virus and AuNZs catalyzes the oxidation of TMB by H_2O_2 and produces a change in color to blue. (a and b) Absorbance at 450 nm and corresponding color change as a function of influenza H1N1 and H3N2 concentration. Adapted with permission from ref.⁸³ Copyright 2018 American Chemical Society.

3.1.2 SERS nanosensors

Raman scattering is the inelastic scattering of a photon that reflects the vibrational transitions of covalent bonds in molecules. Raman spectra represent unique fingerprints of analytes, and the method is becoming increasingly of interest. However, Raman spectroscopy has inherent drawbacks in terms of low sensitivity and high fluorescence interference arising from the weak intensity of inelastic scattering. Since its discovery in the 1970s,^{92, 93} SERS has greatly expanded the applicability of Raman-based methods across various fields. By electromagnetic (EM) nearfield enhancement of both excitation and inelastic scattering transitions of molecules in

1
2
3 hotspots, plasmonic nanomaterials can effectively increase the Raman cross-section of an analyte
4 at their surface vicinity by many order magnitudes.⁹³ This phenomenon is termed SERS. The
5 sensitivity of SERS is proportional to the density of the EM field. In general, the most enhanced
6 EM fields are found within 10 nm of a plasmonic nanostructure. This region (i.e., referred to as a
7 SERS hot spot) can enhance the Raman signal of an analyte by up to 10^{14} .⁹⁴

8
9
10
11
12
13
14
15 The most typical SERS active nanomaterials are Au or AgNPs owing to the tunability of
16 their sizes and shapes and their facile surface functionality.⁹⁵ The LSPR frequency of a NP is an
17 important factor that dictates SERS enhancement. The LSPR position can be finely tuned across a
18 wide spectral range by changing the size and shape of plasmonic nanomaterials. For example, the
19 LSPR band of spherical AuNPs with diameters of 10-80 nm ranges from 520-540 nm.⁹⁶ The
20 anisotropic shape of Au nanorods (AuNRs) with different aspect ratios results in additional, longer
21 wavelength LSPR positions whose position ranges from 650 to 1050 nm.⁹⁶ To achieve the greatest
22 SERS signal, the LSPR of the nanomaterials should spectrally match the excitation laser
23 wavelength.⁹⁷ For this reason, the anisotropic shape of AuNRs can support LSPR with intense EM
24 fields (i.e., SERS enhancement) in the NIR region, which is advantageous for allowing SERS
25 measurements with NIR laser excitation (i.e., 785 nm) to minimize autofluorescence background

26
27
28
29
30
31
32
33
34
35
36
37
38
39
40 SERS can be classified as labeled or label-free methods based on the molecular source of
41 the Raman signal. Label-free SERS reflects the intrinsic signals arising from the virus itself. On
42 the other hand, labeled methods rely upon Raman reporters (e.g., malachite green isothiocyanate
43 (MGITC), rhodamine B isothiocyanate (RBITC), 4-aminothiophenol (4-ATP)) that have large
44 Raman cross-sections and high affinity to the plasmonic nanomaterial surface. The specific
45 interaction among platform, targeted virus, and labeled nanomaterials induces SERS readout
46 changes of Raman reporter on developed platform.

1
2
3 Luo et al. synthesized porous carbon film-coated AgNPs as SERS substrates for label-free
4 detection of porcine circovirus type 2 (PCV2), porcine parvovirus (PPV), and porcine
5 pseudorabies virus (PRV).⁹⁸ The porous structure and hydrophobicity of the substrates can increase
6 viral adsorption and facilitate recyclability. Caglayan et al. synthesized AuNR-based SERS
7 substrates to detect potato virus X (PVX).⁹⁹ To enable SERS-based virus detection, the SERS hot
8 spot size should be carefully considered. The relatively large size of intact viruses (~100 nm)
9 makes them difficult to deposit within nanometer-sized SERS hot spots. Recently, a hollow nano-
10 cone-shaped virus-targeting SERS substrate was fabricated by “molecular imprinting” (**Figure**
11 **Figure 3A**).¹⁰⁰ The ~100 nm opening of the hollow nano-cone can accommodate a range of virus
12 sizes (e.g., adenovirus type 5 (Ad5), 60-90 nm; coxsackievirus type 3 (Cv3), 22-30 nm) while
13 simultaneously possessing a high density of hot spots due to the 3D configuration. The authors'
14 termed the approach volume-enhanced Raman scattering (VERS) and achieved reproducible and
15 reliable detection of Ad5 and Cv3. Durmanov et al. synthesized porous Au nanofilms by electron
16 beam physical vapor deposition and used them for the detection of rabbit myxomatosis virus
17 (MYXV), canine distemper virus (CDV), tobacco mosaic virus (TMV), and PVX.¹⁰¹ The structure
18 of the synthesized substrate has ~300 nm pore-like nano-cavities and indentations that allow for
19 target virus (100~300 nm) capture in the vicinity of the SERS hot spots. Target viruses were
20 successfully detected using this SERS substrate without any recognition elements and
21 differentiated by linear discriminant analysis (LDA). Chang et al. fabricated inverted triangular
22 Au nano-cavities with various indentation depths to entrap AdV, influenza A virus H1N1, and
23 encephalomyocarditis virus (EMCV) (**Figure 3B**).¹⁰² Different sizes and nano-cavity dimensions
24 were fabricated and tested with the three viruses. The substrate with a matching cavity entrapment
25 size to the viruses successfully entrapped them into nano-cavities and induced their SERS spectra.
26
27
28
29
30
31
32
33
34
35
36
37
38
39
40
41
42
43
44
45
46
47
48
49
50
51
52
53
54
55
56
57
58
59
60

Using the best-fitting SERS substrate, the detectable concentration for AdV and EMCV was 10^6 PFU/mL, while for H1N1 it was 10^4 PFU/mL.

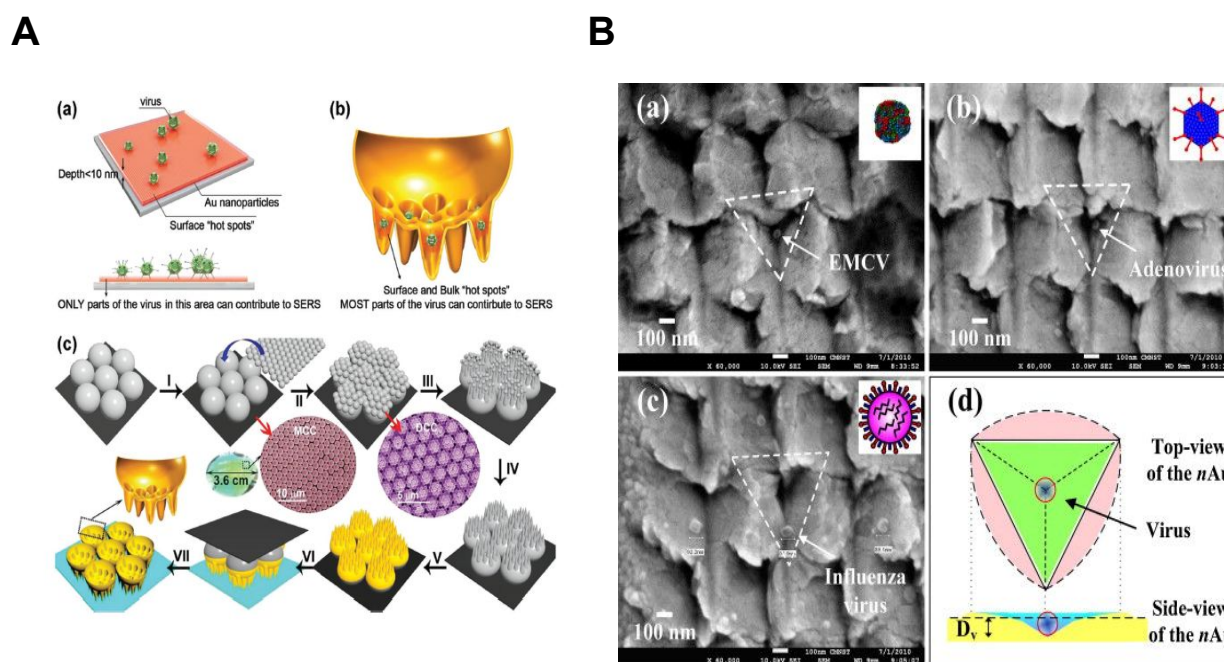


Figure 3. Fabricated SERS substrates for virus detection. (A) Au hollow nano-cone-shaped SERS substrate with indentations for sensitive SERS hot spots inspired by “molecular printing”. Adapted with permission from ref.¹⁰⁰ Copyright 2019 Wiley-VCH. (B) Inverted triangular Au nano-cavity arrays with different sizes for EMCV, AdV, and influenza virus H1N1. Adapted with permission from ref.¹⁰² Copyright 2011 Elsevier B. V.

To capture specific viruses, plasmonic nanomaterials can be functionalized with recognition elements such as aptamers, antibodies, peptides, and chemical molecules. Recently, cell receptor angiotensin-converting enzyme 2 (ACE2) has been used as a recognition element for SARS-CoV-2 owing to its high affinity to spike protein receptor-binding domain (S RBD). Yang et al. fabricated ACE2-functionalized gold nanoneedles for selective capture and SERS detection of SARS-CoV-2. This platform exhibited a LOD of 80 copies/mL.¹⁰³ Similarly, Ag nanorods (AgNRs) functionalized with ACE2 enabled rapid SERS detection of SARS-CoV-2 in environmental specimens.¹⁰⁴ In this result, SERS peaks arising from ACE2 were quenched by hydrophilic interaction at ACE2/RBD when SARS-CoV-2 spike protein bound to the substrates.

1
2
3 The specific interaction and high equilibrium association constants for the antibody-
4 antigen complex enhance sensitivity and specificity.¹⁰⁵ Moon et al. synthesized antibody
5 conjugated AuNPs using a gold binding peptide (GBP) and used them for labeled SERS detection
6 of influenza A virus H1N1.¹⁰⁶ GBP can be attached to the surface of AuNP and the Fc (Fragment,
7 crystallizable) region of an antibody. The target virus was selectively captured on an antibody-
8 conjugated glass slide. Detection was then enabled by the attachment of RBITC functionalized
9 AuNPs with the Raman signal of RBITC used to indicate virus detection. The sensitivity of this
10 substrate was improved to a LOD of 4.1×10^3 TCID₅₀/mL by adding a signal-enhancing Ag layer.
11 Using the same principle, a two-dimensional Au@Ag core-shell NP array was synthesized as a
12 SERS substrate for sensitive detection of influenza A virus nucleoprotein.¹⁰⁷ The SERS signal of
13 this array was $\sim 4 \times$ greater than that of a flat Au film. Sandwich formation with 4,4'-
14 thiobisbenzenethiol-coated AuNPs in the presence of influenza A virus nucleoprotein showed a
15 LOD of 6 TCID₅₀/mL.
16
17
18
19
20
21
22
23
24
25
26
27
28
29
30
31
32

33 Recently, oseltamivir hexylthiol (OHT) and MGITC functionalized AuNPs were utilized
34 for SERS detection of oseltamivir-resistant virus.¹⁰⁸ The wide use of oseltamivir (Tamiflu) to
35 prevent influenza virus infection has led to the emergence of oseltamivir-resistant virus strains. It
36 was found that OHT exhibited a higher affinity for oseltamivir-resistant (pH1N1/H275Y mutant)
37 viruses than for the wild-type virus.¹⁰⁹ Using MGITC functionalized AuNPs, pH1N1/H275Y
38 mutant viruses were successfully detected due to the SERS MGITC signal enhancement that
39 occurs from analyte-mediated AuNP aggregation. Even with the high concentration of wild-type
40 viruses, the functionalized AuNPs were able to selectively detect pH1N1/H275Y mutant viruses.
41 Moreover, these functionalized AuNPs can be used for mutant virus diagnosis in complex nasal
42 fluid and saliva specimens with concentrations as low as 1 PFU.¹¹⁰
43
44
45
46
47
48
49
50
51
52
53
54
55
56
57
58
59
60

1
2
3 Aptamer-functionalized SERS substrates can also be utilized to selectively detect the virus.
4
5 Recently, Chen et al. synthesized DNA aptamer functionalized Au nanopopcorn with high affinity
6
7 to the spike protein of SARS-CoV-2.¹¹¹ A Raman reporter, cyanine 3 (Cy3), was attached to the
8
9 aptamer and situated close to the surface of the substrate. The aptamer was designed to be released
10
11 when it binds to the spike protein of SARS-CoV-2. The release of aptamer from the substrate then
12
13 leads to a decrease in the Cy3 Raman signal. This platform successfully detected SARS-CoV-2
14
15 lysate with a LOD of <10 PFU/mL within 15 mins. Aptamer RHA 0385 showed a high affinity
16
17 for influenza A viruses of the H1N1, H3N2, and H5N1 strains.¹¹² For the detection of influenza
18
19 viruses, the SERS substrate was synthesized by covering a thick layer of Ag granules on a silicon
20
21 plate.¹¹³ A SERS substrate functionalized with primary aptamer (RHA 0385) was used to capture
22
23 the virus. Following capture, the secondary aptamer, Cy3 labeled RHA 0385, formed a sandwich
24
25 complex in the presence of the influenza virus. The high Raman signal of Cy3 enabled sensitive
26
27 viral detection.
28
29
30
31
32

33 For simple point-of-care (POC) or point-of-use (POU) virus detection, a SERS-based
34
35 lateral flow (LF) strip has proven effective.¹¹⁴⁻¹¹⁷ LF strips are an attractive sensor platform that
36
37 relies upon capillary force-driven sample movement through a stationary membrane. Traditionally,
38
39 targeted analytes can be captured by immobilized recognition elements and detected by the visual
40
41 color of colloidal samples such as AuNPs. SERS-based LF strips can selectively capture analytes
42
43 with high sensitivity and easy operation.¹¹⁴ Xiao et al. synthesized novel core-shell structured
44
45 plasmonic NPs ($\text{AuAg}^{4\text{-ATP}}\text{@AgNPs}$) consisting of a double-layered shell of Au and Ag and an
46
47 AgNP core that was functionalized with 4-ATP as a Raman reporter.¹¹⁵ To capture influenza A
48
49 virus H7N9, a H7N9 monoclonal antibody was conjugated to the $\text{AuAg}^{4\text{-ATP}}\text{@AgNPs}$ and the test
50
51 line (TL) on the strip while goat anti-mouse IgG was used for the control line (CL). High sensitivity
52
53
54
55
56
57
58
59
60

1
2
3 detection of H7N9 was achieved using these SERS-based LF strips with a LOD of 0.0018
4 hemagglutination unit (HAU). Using the same method, selective and sensitive detection of PRV
5 was realized with a detection limit of 5 ng/mL.¹¹⁶ Further, a magnetic SERS-based LF strip was
6 developed to detect influenza A virus H1N1 and AdV in biological samples.¹¹⁷ Magnetic NPs have
7 the advantage of facile magnetic enrichment and the separation of target viruses from potentially
8 interferent constituents without pretreatment. Wang et al. synthesized iron oxide and Ag core-shell
9 NPs ($\text{Fe}_3\text{O}_4@Ag$ NPs) for such a SERS application (**Figure 4**).¹¹⁷ $\text{Fe}_3\text{O}_4@Ag$ NPs were
10 functionalized with 5,5-dithiobis-(2-nitrobenzoic acid) as a Raman reporter, and two specific
11 antibodies to H1N1 and AdV were conjugated to the particles. $\text{Fe}_3\text{O}_4@Ag$ NPs were incubated in
12 H1N1- and AdV-spiked human whole blood, serum, and sputum. The conjugates were then
13 magnetically separated and re-suspended in the buffer for SERS/LF strip-based detection. Two
14 separate test lines for H1N1 and AdV each with virus specific antibodies were used. Upon addition
15 of suspension onto the LF strip, the two test lines are positive in the presence of each virus. The
16 LODs were 50 and 10 PFU/mL for H1N1 and AdV, respectively. The stability of the platform was
17 tested in 0.1 M PBS over a pH range of 5.0-9.0. There was no significant effect of pH on detection
18 performance.

19
20
21
22
23
24
25
26
27
28
29
30
31
32
33
34
35
36
37
38
39
40 SERS was recently coupled with an enzyme-catalyzed immunoassay for virus detection.
41 In the presence of the target virus, an enzyme reaction product induces NP aggregation and
42 facilitates the generation of a strong SERS signal. Zhan et al. detected respiratory syncytial virus
43 (RSV) using an HRP-induced catalytic reaction and SERS. HRP catalyzes the oxidation of TMB
44 by H_2O_2 to TMB^+ .¹¹⁸ Through constructing a sandwich complex between HRP conjugated
45 antibody and RSV, TMB was converted into a positively charged reactant that electrostatically
46
47
48
49
50
51
52
53
54
55
56
57
58
59
60

1
2
3 binds to the negatively charged AgNPs. Following complex formation, AgNP aggregation
4
5 produced strong SERS signals for oxidized TMB. The LOD of this method was 0.05 pg/mL.
6
7

8 Overall, both label-free and labeled SERS show great potential for sensitive virus detection.
9
10 Label-free SERS reflects the intrinsic signal of the virus itself but exhibits lower sensitivity. We
11
12 anticipate that virus size-oriented design of label-free SERS substrates that enable effective
13
14 deposition of the virus within dense SERS hot-spots will be of growing research focus as a means
15
16 to increase SERS intensity. Moreover, advanced data analytics should help virus discrimination
17
18 and quantification in more complex systems.¹¹⁹ Labeled SERS takes advantage of the strong signal
19
20 of Raman reporter molecules, but requires an additional surface functionalization process.
21
22 Different Raman reporters and recognition elements should be modified for the detection of
23
24 multiple viruses.¹¹⁷ Raman instrumentation can be costly in a bench-top format. However, there
25
26 are a field-deployable formats (i.e., portable Raman instruments) that come with great mobility
27
28 and lower prices. In addition, it is relatively simpler to operate than current PCR-based assays
29
30 since it does not require any reagents to run the assay. It would essentially reduce the cost of
31
32 maintenance and analysis. In future studies, the expansion of multiplex labeling should be
33
34 improved. In addition, SERS has exhibited great compatibility with POC/POU platforms such as
35
36 LF. The stability of SERS substrates for real sample applications and the costs should be
37
38 considered in future studies.
39
40
41
42
43
44
45
46
47
48
49
50
51
52
53
54
55
56
57
58
59
60

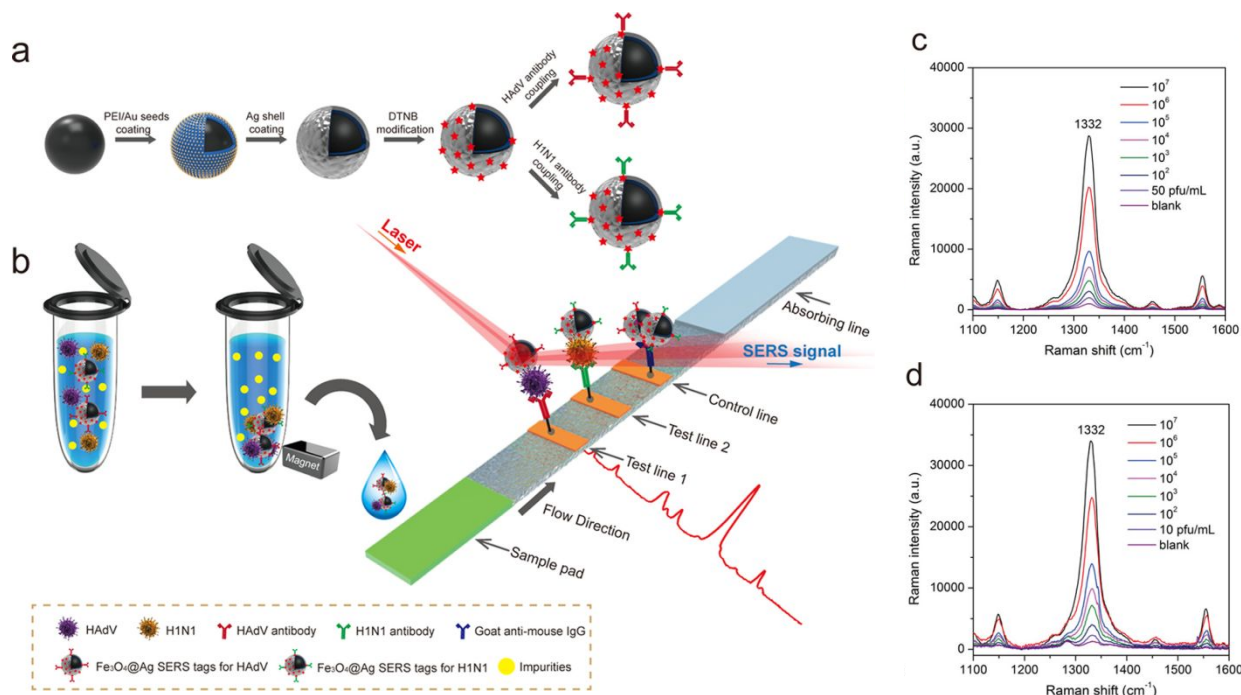


Figure 4. SERS detection of the virus. (a) Two antibody-conjugated Fe₃O₄@Ag core-shell NPs were synthesized for the detection of H1N1 and AdV. (b) Dual SERS detection was enabled by a magnetic SERS-based LF strip. H1N1 and AdV were selectively separated from impurities via a magnetic field. (c and d) SERS spectra of test lines 1 and 2 with different concentrations of H1N1 and AdV. Adapted with permission from ref.¹¹⁷ Copyright 2019 American Chemical Society.

3.1.3 Fluorometric nanosensors

Fluorescent nanomaterials can induce down-conversion or up-conversion fluorescence emission, mediated by single-photon or multi-photon excitation and emission transitions between their electronic states. Therefore, fluorescent nanomaterials can be engineered as fluorometric nanosensors or nanoprobe to detect viruses or other bio-markers based on their interfacial interaction-modulated fluorescence emission signal changes.¹²⁰ For example, fluorescence can be quenched when an analyte attaches to a fluorescent NP and disrupts the non-radiative transfer of energy, referred to as fluorescence resonance electron transfer (FRET). On the other hand, the interaction between the analyte and the fluorescent NPs can enhance fluorescence emission by minimizing the quenching pathway associated with the surrounding environment. Fluorescent

1
2
3 single isomers such as 6-carboxylfluorescein (6-FAM) can be coupled with NPs to develop
4
5 fluorometric nanosensors.¹²¹ Recently, single-walled CNT (SWCNT) fluorometric nanosensors
6
7 were developed for SARS-CoV-2 detection.¹²² The SWCNTs were functionalized with ACE2 for
8
9 high affinity to SARS-CoV-2 spike protein, leading to fluorescence quenching. The presence of
10
11 SARS-CoV-2 S RBD resulted in an increase in fluorescence within 90 mins with a LOD of 12.6
12
13 nM.
14
15

16
17 The LSPR of plasmonic NPs can be applied to fluorometric virus sensing approaches.
18
19 Fluorescence signal intensity can be controlled by coupling plasmonic NPs to fluorescent
20
21 particles.¹²³ Numerous FRET-based sensors have been developed for virus detection. Shojaei et
22
23 al. detected citrus tristeza virus (CTV) using CdTe QDs coupled with AuNPs.¹²⁴ Formation of an
24
25 immuno-complex between CTV protein conjugated AuNPs and antibody-conjugated QDs that
26
27 have a high affinity to CTV protein quenched the fluorescent signal. By competitively replacing
28
29 AuNPs with free CTV protein in the presence of CTV, the fluorescent signal increased. The
30
31 authors found that an AuNP and QD molar ratio of 1:6.5-8.5 showed the highest FRET efficiency.
32
33 The detection assay showed a LOD of 0.13 $\mu\text{g/mL}$. Takemura et al. also applied the LSPR from
34
35 AuNPs to enhance fluorescence from quaternary alloy CdSeTeS QDs.¹²⁵ Via the same antigen-
36
37 antibody interaction, AuNPs and QDs were attached to influenza A virus H1N1. LSPR-induced
38
39 immunofluorescence enhancement was ~ 3.6 fold compared to QDs alone and enabled sensitive
40
41 detection of H1N1 with a LOD of 0.03 and 0.4 pg/mL in deionized water and human serum,
42
43 respectively. In addition to AuNPs, CNTs combined with AuNPs have a synergistic effect on
44
45 fluorescence enhancement.¹²⁶ Au-decorated CNTs (AuCNTs) exhibit a unique platform to work
46
47 as a combined signal enhancer and transducer. Using antibody conjugated AuCNTs and CdTe QDs
48
49 as a plasmon-assisted fluoro-immunoassay (PAFI) platform, influenza A H1N1 and H3N2 viruses
50
51
52
53
54
55
56
57
58
59
60

1
2
3 were detected. The minimum detection concentration was 0.1 pg/mL. For the clinically isolated
4
5 viruses, the LOD was 50 PFU/mL.
6

7
8 Many studies have employed plasmonic NPs with LSPR to control the intensity of the
9
10 fluorescent signal. The enhancement of fluorescence signals by such plasmonic NPs highly
11
12 depends on the distance between the plasmonic NPs and QDs. It has been observed that
13
14 fluorescence can be enhanced at a distance of 10-15 nm between them and can be quenched at a
15
16 distance of <5 nm.¹²⁷ Using the principle of fluorescence quenching by steric hindrance between
17
18 fluorescent and plasmonic NPs, a highly sensitive virus detection biosensor was developed (**Figure**
19
20 **5A**).¹²⁸ Fluorescent inorganic QDs (CdZnSeS/ZnSeS QDs) and AuNPs were linked by an 18
21
22 amino acid peptide chain. This peptide was functionalized with specific antibodies against
23
24 influenza A virus H1N1. Following virus attachment to the peptide chain linker between the QDs
25
26 and AuNPs, the fluorescence intensity was gradually quenched. This tunable LSPR-assisted
27
28 fluorometric detection approach achieved a detection limit of 17.02 fg/mL.
29
30
31
32

33
34 Many biological samples contain impurities that may deteriorate detection efficiency or
35
36 impede fluorescence emission, resulting in unreliable results. Magnetic NPs can be applied to
37
38 separate the analyte from impurities in the sample using an external magnetic field. Multiplex
39
40 detection of EV71 and coxsackievirus B3 (CVB3) using antibody-conjugated magnetic nanobeads
41
42 and CdSe QDs was successfully used for clinical swab samples.¹²⁹ Two specific antibodies to
43
44 EV71 and CVB3 were used to functionalize the magnetic nanobeads and two colored QDs with
45
46 different emission wavelengths (QDs 525 and 605) were employed. With both viruses present,
47
48 strong fluorescence signals from QDs 525 and 605 were simultaneously observed with LODs of
49
50 858 and 809 copies/500 μ L for EV71 and CVB3, respectively. Using Au and magnetic hybrid NPs
51
52 coupled with QDs, a LSPR-amplified magnetofluoroimmunoassay (MFIA) for detecting NoV was
53
54
55
56
57
58
59
60

1
2
3 reported (**Figure 5B**).¹³⁰ Hybrid NPs conjugated with antibodies that have a high affinity to NoV
4 enabled virus capture from human feces. Complexes of NoV-captured hybrid NPs and antibody
5 conjugated L-Glutathione-capped CdSeS core QDs were successfully separated from human feces
6 by a magnetic field. This approach provided an LSPR-amplified fluorescence signal only in the
7 presence of NoV with a LOD of 0.48 pg/mL.
8
9

10
11
12
13
14 For simplicity and rapid detection, a fluorescent immunochromatographic strip test (FICT)
15 assay has been developed. The strip assay uses capillary forces, as previously described, to move
16 the sample through a stationary membrane. At the TL and CL, anti-virus antibodies and anti-mouse
17 immunoglobulin are conjugated. At the TL, in the presence of a target virus, fluorescent NPs
18 conjugated with anti-virus antibodies form a sandwich complex with the virus and the fluorescence
19 intensity at the TL and CL were measured, and the TL/CL ratio was used for quantitative analysis.
20 Recently, FICT assays were developed for influenza A virus H1N1-confirmed patients.^{131, 132}
21 Using commercially available Europium NPs, the reported LOD of the assay was below 20
22 HAU/mL. The assay also showed 85.3% sensitivity and 100% specificity for patient diagnosis.
23 Antibodies to influenza H7 subtype virus were developed for better selectivity and used for
24 detecting H7N1 and H7N7.¹³³ The FICT assay was only positive for H7N1 and H7N7 with a LOD
25 of 40 HAU/mL and was negative for H1N1 and H5N3. Additionally, to improve the system
26 detection sensitivity, CdSe/CdS/ZnS QDs were applied instead of Europium NPs. The QDs were
27 functionalized with 3-mercaptopropionic acid to make them water-soluble. The higher quantum
28 yield and fluorescence efficiency of CdSe/CdS/ZnS QDs-linked FICT assay showed lower LODs
29 (2.5 HAU/mL for H1N1 virus and 0.63 HAU/mL for H3N2 virus).¹³²
30
31
32
33
34
35
36
37
38
39
40
41
42
43
44
45
46
47
48
49
50

51 Aptamer functionalized QDs have also been used for virus detection. A QD embedded target-
52 responsive hydrogel sensor functionalized with aptamer was developed to detect influenza A virus
53
54
55
56
57
58
59
60

1
2
3 H5N1.¹³⁴ Polymer crosslinked aptamer hydrogel with a high affinity to H5N1 surface
4 hemagglutinin was synthesized and terminated with QD quenchers. The hydrogel protects the QDs
5 from external interference. Using single-strand DNA (ssDNA) terminated QDs, H5N1 was
6 detected through the interaction between aptamer-quencher and ssDNA-QD. In the presence of
7 H5N1, aptamer was attached to the virus and the fluorescence signal was observed from ssDNA-
8 QD. This method showed the lowest detection limit of 0.4 HAU. Weng and Neethirajan reported
9 the detection of NoV enabled by aptamer functionalized 6-FAM coupled with multi-walled CNTs
10 (MWCNTs) or GO.¹²¹ Carbon-based nanomaterials were used as fluorescence quenchers of FRET.
11 When 6-FAM terminated aptamer with high affinity to NoV was bound with MWCNTs or GO in
12 the absence of NoV, the fluorescence signal was quenched. The aptamer can be released when it
13 binds to NoV, leading to fluorescence recovery. The reported LODs were 4.4 and 3.3 ng/mL when
14 MWCNTs and GO were used, respectively.

15
16
17
18
19
20
21
22
23
24
25
26
27
28
29
30
31 The surveyed literature suggests that fluorometric nanosensors can successfully detect
32 viruses. We anticipate that a growing number of nanomaterials that can effectively quench
33 fluorescence signals or improve FRET efficiency will be developed. Additionally, due to the low
34 quantum yield and photobleaching issue of some fluorescent NPs, the search of synthesis of low-
35 cost, stable, and efficient nanomaterials is an ongoing area of research focus.¹³⁵⁻¹³⁸
36
37
38
39
40
41
42
43
44
45
46
47
48
49
50
51
52
53
54
55
56
57
58
59
60

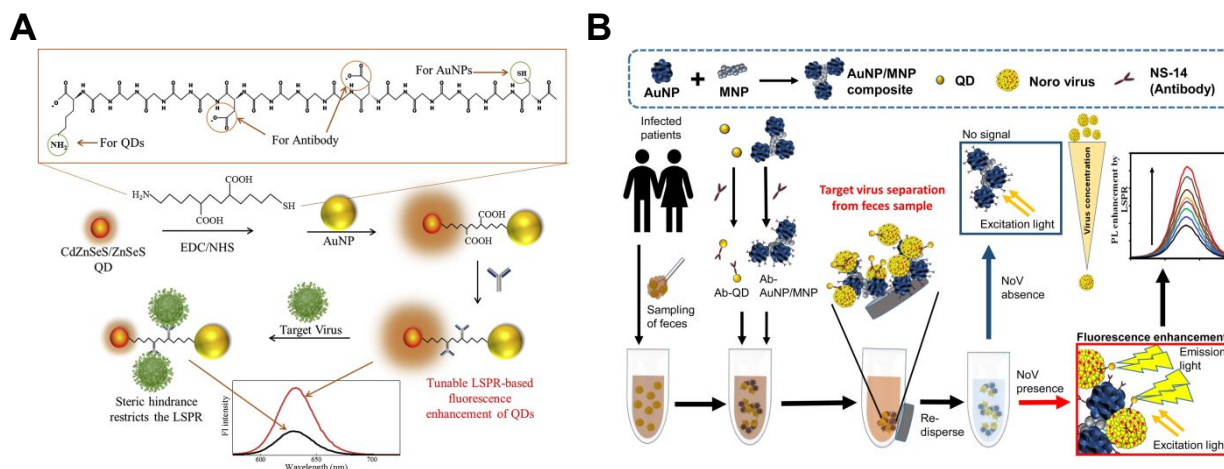


Figure 5. Fluorometric detection of the virus (A) AuNPs and QDs were linked through the peptide chain to induce tunable LSPR-based fluorescence enhancement of QDs. The peptide chain was functionalized with the antibody and fluorescence was quenched by steric hindrance when the target virus was attached to this chain. Adapted with permission from ref.¹²⁸ Copyright 2020 Elsevier B. V. (B) LSPR-amplified magnetofluoroimmunoassay (MFIA) was used for the detection of NoV separated from human feces. Au/magnetic NPs (AuNP/MNP composite) and QDs were functionalized with antibodies to capture NoV. Complexes of NoV-captured AuNP/MNP composite and QDs were separated from human feces and enriched by a magnetic field. The concentration of NoV was reflected by fluorescence enhancement. Adapted with permission from ref.¹³⁰ Copyright 2019 Elsevier B. V.

3.2 Electrical nanosensors

Electrical nanosensors employ conductive nanomaterials such as carbon-based materials (e.g., CNTs and graphene), metals, and metal oxides (e.g., titanium oxide (TiO₂), zinc oxide (ZnO)), polymers, and other inorganic nanomaterials,¹³⁹⁻¹⁴¹ as the signal transducer to convert interfacial analyte binding events into electrical voltage or current signals. According to the underlying signal transduction mechanisms, electrical nanosensors can be primarily classified into electrochemical nanosensors, chemiresistor-based nanosensors, and field-effect transistor based nanosensors.¹⁴¹

3.2.1 Electrochemical nanosensors

As a prominent type of electrical nanosensors for virus detection, electrochemical nanosensors exploit the highly sensitive dependence of interfacial electrochemical processes on

1
2
3 the analyte binding events at the nanomaterials-modified microelectrode surface for signal
4 transduction. Electrochemical sensors are suitable for real-time virus detection because they can
5 potentially achieve high sensitivity, good selectivity, low- device cost, compact instrumentation,
6 high portability, and fast analysis.¹⁴²
7
8
9
10
11

12 To date, electrochemical nanosensors primarily utilize carbon-based nanomaterials¹⁴³ and
13 metal/metal oxide NPs.¹⁴⁴ Usually, these nanomaterials are used to modify electrodes for better
14 capture of the target virus and for the amplification of the transducer signal. The most straight-
15 forward approach for virus detection using electrochemical nanosensors is the direct capture of
16 viruses on the electrode surface and the subsequent measurement of electrical signal changes.
17 Employing an embedded vertically aligned carbon nanofiber nanoelectrode array (NEA), Madiyar
18 et al. captured vaccinia virus particles and measured virus concentration based on the
19 electrochemical signal change (**Figure 6A**).¹⁴⁵ The virus particles were first captured by the NEA
20 using a low voltage and the interfacial impedance changes at the electrode were subsequently
21 measured. A LOD of $\sim 2.58 \times 10^3$ particles/mL was reported. This rapid, reversible, and label-free
22 detection method exhibited potential for future study. In addition to pre-immobilizing
23 nanomaterials on the electrode, we can simultaneously introduce the NPs and the virus analytes to
24 the sensor surface to improve detection performance. Sepunaru et al. found that in the presence of
25 the influenza virus, AgNPs can be adsorbed on a carbon electrode efficiently at open circuit
26 potential due to the 'sticky' property of the H1N1, which comes from the adsorption of viral
27 proteins to electrode surface.¹⁴⁶ The frequency and amplitude of the current spikes showed a high
28 linear correlation with virus concentration. This method enabled rapid detection of influenza virus
29 H1N1 at the sub pM level.
30
31
32
33
34
35
36
37
38
39
40
41
42
43
44
45
46
47
48
49
50
51
52
53
54
55
56
57
58
59
60

1
2
3 Unfortunately, direct viral capture methods cannot ensure specific binding of the target
4 virus and changes in the electrochemical signal are not always strong enough to be detectable. For
5 these issues, recognition elements can be used to modify the electrode surface.¹⁴⁷ Antibodies are
6 the most commonly used recognition elements for this purpose. To date, many researchers have
7 adapted antibody-modified electrochemical biosensors for virus detection.^{148, 149} Wang et al.
8 fabricated AuNP-based micro/nano hybrid-structured sensing electrodes to detect odontoglossum
9 ringspot virus (ORSV).¹⁴⁸ The electrodes were first modified with a self-assembled monolayer
10 (SAM) of anti-ORSV antibodies and electrochemical impedance spectroscopy (EIS) changes were
11 monitored for ORSV quantification. This method has achieved a low LOD (0.238 ng/ml).
12 Similarly, a microfluidic immunosensor has been successfully developed for simultaneous sensing
13 of influenza A virus H1N1, H5N1, and H7N9 (**Figure 6B**).¹⁵⁰ ZnO nanorods (ZnONRs) on the
14 polydimethylsiloxane surface in the sensing region enhanced the sensitivity of the amperometric
15 signal and the LOD was as low as 1 pg/mL for each virus. Recently, Hashemi et al. developed an
16 electrochemical diagnostic kit by coating a layer of GO with sensitive chemical compounds (8-
17 hydroxyquinoline, 1-ethyl-3-(3-dimethylaminopropyl) carbodiimide (EDC), and N-
18 hydroxysuccinimide (NHS)) along with gold nanostars (AuNSs).¹⁵¹ Differentiable fingerprint
19 DPV patterns of SARS-CoV-2 and animal virus glycoproteins can be obtained at different voltage
20 positions. The sensor demonstrated a LOD of 1.68×10^{-22} $\mu\text{g/mL}$ toward SARS-CoV-2 in biological
21 media. Peptides are another commonly used recognition element in electrochemical sensors for
22 virus detection. Zhao et al. developed a sandwich type electrochemical sensor for NoV using both
23 aptamer and peptide recognition elements.¹⁵² Aptamer was modified on magnetic nanocomposites
24 while peptides were functionalized on the surface of an AuNP modified electrode. The sensor
25 showed high sensitivity with a LOD of 0.8 copy/mL. Baek et al. developed a peptide functionalized
26
27
28
29
30
31
32
33
34
35
36
37
38
39
40
41
42
43
44
45
46
47
48
49
50
51
52
53
54
55
56
57
58
59
60

1
2
3 electrochemical sensing platform for NoV.¹⁵³ AuNP-decorated tungsten disulfide nanoflowers
4 (WS₂NF/AuNP) were modified by peptides and specifically capture NoV. The impedance is
5 increased through hindrance of charge transfer between the working electrode and redox species
6 with a LOD of 2.37 copies/mL.
7
8
9
10
11

12 To enhance the electrochemical signal, labels (primarily enzymes) have been used to
13 produce or consume an electroactive cofactor that can be monitored at the electrode interface.¹⁰⁵
14 HRP is a commonly used enzyme label in electrochemical sensors. HRP conjugated antibodies are
15 attracted to the electrode surface in the presence of viruses. TMB on the surface of the electrode
16 can be oxidized by HRP, resulting in an electrochemical redox current (**Figure 6B**).¹⁵⁰ Glucose
17 oxidase (GOD) and alkaline phosphatase are two other frequently used enzyme labels.^{154, 155}
18 Conjugated GOD is an extraordinary electrochemical biocatalyst for the reduction of ionic β -
19 cyclodextrin-ferrocene and has been successfully applied to detect avian leukosis virus (ALV).¹⁵⁶
20 In addition to redox labels, electrochemiluminescence (ECL) labels are also commonly used for
21 virus detection.¹⁵⁷ Luo et al. successfully detected influenza A virus H9N2 by encapsulating
22 Ru(bpy)₃²⁺ in silica nanoparticles (RuSi NPs) and then modifying these NPs with a polyclonal
23 antibody.¹⁵⁷ The ECL signals were amplified about 10³-fold compared with the same concentration
24 of Ru(bpy)₃²⁺. Antibody-modified magnetic nanobeads were used to capture and separate virus
25 conjugated RuSi NPs and the ECL immunosensor achieved ultrasensitive detection of 14 fg/mL
26 for H9N2. Combinations of labels and nanomaterials can significantly improve detection
27 sensitivity.
28
29
30
31
32
33
34
35
36
37
38
39
40
41
42
43
44
45
46
47
48

49 To expand the application of electrical nanosensors for virus detection, some researchers
50 have focused more on sensing viral nucleic acid (DNA or RNA) than intact viruses.
51 Electrochemical DNA/RNA sensing techniques can be used for virus identification and
52
53
54
55
56
57
58
59
60

1
2
3 quantification with high sensitivity and specificity. Often, ssDNA sequences and different kinds
4 of indicators are modified on nanomaterials adhered to the electrode surface.^{158, 159} When a
5 complementary target sequence approaches, the redox reaction on the indicators will cause the
6 change in the electrochemical signal and the target viral sequence can be detected. Tahir et al.
7 successfully detected agrovirus DNA in infected plant leaves using methylene blue (MB) as a
8 redox indicator.¹⁶⁰ CNT-based copper NP composites were used to immobilize probe DNA. When
9 DNA hybridization happened, the electroactivity of MB solution decreased and the reduction in
10 current was used for quantification. Li et al. developed a DNA-assisted magnetic reduced graphene
11 oxide (mrGO)-copper nanocomposite (CuNCs) for the detection of hepatitis C virus (HCV).¹⁵⁸
12 CuNCs combine with mrGO when probe ssDNA hybridized with target HCV DNA. The indicator,
13 o-phenylenediamine, is oxidized to 2,3-diaminobenzazine in the presence of CuNCs and the
14 electrochemical signal is used to characterize the HCV DNA.
15
16
17
18
19
20
21
22
23
24
25
26
27
28
29

30
31 Nucleic acid-based methods have been also successfully used for SARS-CoV-2 detection.
32 Alafeef et al. developed an electrochemical biosensor using AuNPs functionalized with ssDNA to
33 target SARS-CoV-2 RNA.¹⁶¹ The sensor provided a significant increase in output signal only in
34 the presence of SARS-CoV-2 RNA within <5 min and the LOD was 6.9 copies/ μ L. Using a similar
35 principle, Zhao et al. developed a rapid, accurate, and easy-to-implement electrochemical sensor
36 for SARS-CoV-2 RNA diagnosis.¹⁶² When applied to a clinical specimen, the LOD was 200
37 copies/mL and the detectable ratios for SARS-CoV-2 confirmed patients were even higher than
38 those obtained using RT-qPCR. More recently, Chaibun et al. applied such a sandwich assay for
39 SARS-CoV-2 amplicons from rolling circle amplification.¹⁶³ The probes were functionalized with
40 redox-active labels. The one-step sandwich hybridization assay could detect as low as 1 copy/ μ L
41 of genes within 2 h. The developed sensor gave a 100% concordance result with PCR-based
42
43
44
45
46
47
48
49
50
51
52
53
54
55
56
57
58
59
60

technique when evaluating 106 clinical samples. In addition to nucleic acid, the other components of viruses such as proteins¹⁶⁴ and peptides¹⁶⁵, can also be detected using similar methods. For example, Kaushik et al. developed a functionalized interdigitated micro-electrode Au array for ZIKV protein detection.¹⁶⁴ The ZIKV protein could bind with ZIKV-specific envelop protein antibody, and EIS was used to measure the electrical impedance responses of the developed sensing chip with a LOD of 10 pM. The detection of nucleic acid and protein greatly expanded the applicability of virus detection through electrochemical nanosensors.

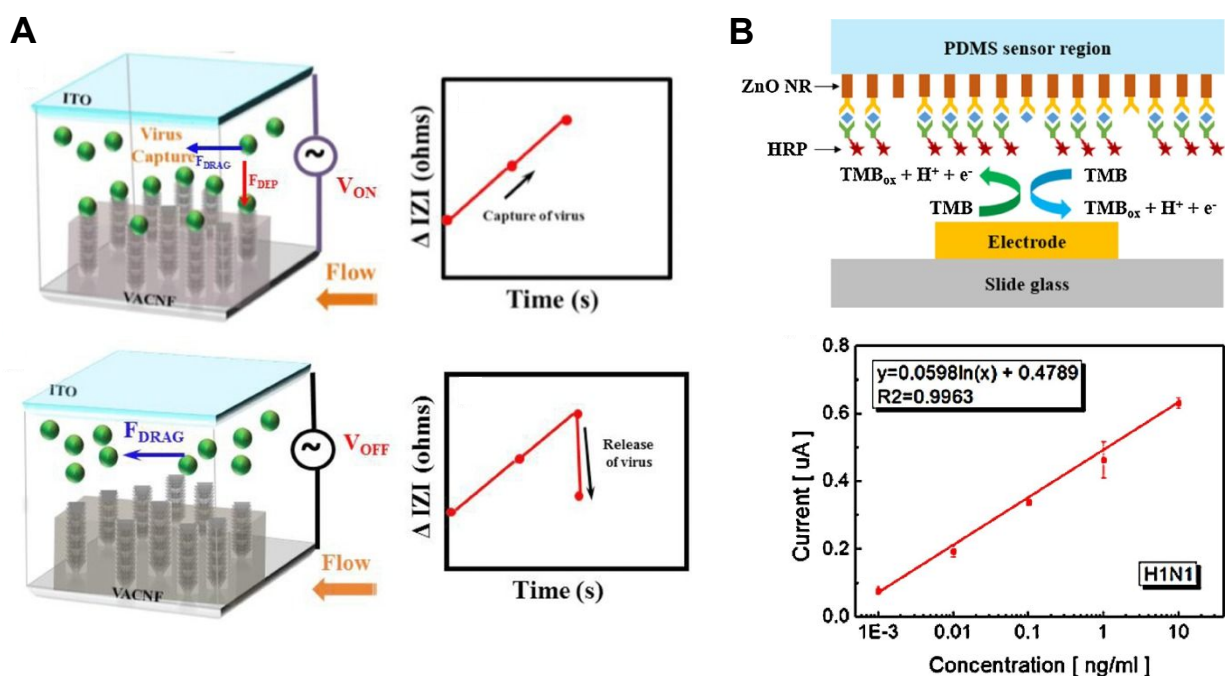


Figure 6. Electrochemical detection of viruses. (A) Direct virus particles capture using carbon nanoelectrode arrays when the voltage is on and off. Adapted with permission from ref.¹⁴⁵ Copyright 2017 Wiley-VCH. (B) TMB-HRP oxidation mechanism on the electrochemical immunosensor working electrode and the calibration curve of the H1N1 sensor at different concentrations. Adapted with permission from ref.¹⁵⁰ Copyright 2016 Elsevier B.V.

3.2.2 Chemiresistor-based nanosensors

Chemiresistors-based nanosensors employ nanomaterials with chemosensitive resistance to convert analyte adsorption-desorption events at the sensor surface into sensor resistance changes

1
2
3 for electrical signal readout. In this way, chemiresistor nanosensors can detect viral analytes in
4
5 real-time.
6

7
8 One-dimensional nanostructures such as SiNWs, conducting polymer NWs, and CNTs are
9
10 the most often used nanomaterials in chemiresistors.¹⁴¹ When used for virus detection, recognition
11
12 elements are essential for most chemiresistors since viruses alone seldom change the resistance
13
14 without a recognition element. Like other types of nanosensors we discussed earlier, antibodies
15
16 are the most often used recognition elements in chemiresistors. Shirale et al. developed
17
18 chemiresistive immunosensors based on single polypyrrole (Ppy) NWs to detect bacteriophages
19
20 T7 and MS2 through immobilization of anti-T7 or anti-MS2 antibodies (**Figure 7A**).¹⁶⁶ Ppy NWs
21
22 were used to connect a pair of Au electrodes and modified with different antibodies. A change in
23
24 sensor resistance was observed upon exposure to different concentrations of spiked bacteriophages
25
26 and the LOD reached 10^{-3} PFU in 10 mM PBS for both targets. Cucumber mosaic virus (CMV)
27
28 can be detected via similar approach.¹⁶⁷ However, antibodies are sensitive to environmental
29
30 condition changes (such as pH, temperature, enzymes, and other substances) and may not be
31
32 applicable for biosensing under field conditions.¹⁶⁸ Hence, some researchers have used other
33
34 recognition elements in chemiresistors. Wasik et al. developed a heparin-functionalized CNT-
35
36 based chemiresistor for DENV.¹⁶⁹ In their study, they used heparin as the recognition element since
37
38 it is stable during storage under adverse conditions. In the presence of heparin, DENV could be
39
40 captured on the surface of CNT and elicited an increase in resistance.
41
42
43
44
45
46

47 Nucleic acid can also be used to determine viruses in chemiresistors. Prior studies have
48
49 found that DNA probe can be non-covalently attached to CNT sidewalls due to their strong van
50
51 der Waals attraction to hexagonal carbon structures.¹⁷⁰ Fu et al. developed a chemiresistor based
52
53 on CNTs to detect the DNA sequence of influenza A virus H5N1 (**Figure 7B**).¹⁷¹ In this biosensor,
54
55
56
57
58
59
60

the CNTs were first functionalized with DNA probe sequences. The DNA probe sequences significantly increase in the relative resistance for CNTs, which provide high initial resistance. When the target complementary DNA sequences were hybridized, a significant decrease in device resistance was observed. The resistance change maintained a continuous downward trend when the concentration ranged from 20 pM to 20 nM.

The resistance of virus-binding chemiresistors can be affected by some other substances (e.g., proteins) as has been reported by Bhasin et al.¹⁷² In their work, they found that the high resistance of filamentous M13 virus-binding chemiresistors could be decreased in the presence of human serum albumin (HSA) and could be used for the quantification of HSA in the system. It is a promising work for the detection of protein. Nevertheless, we note that the presence of co-contaminants might significantly affect the viral chemiresistor electrical signal. If such a method was adopted, it would be important to consider the chemical properties of the solution.

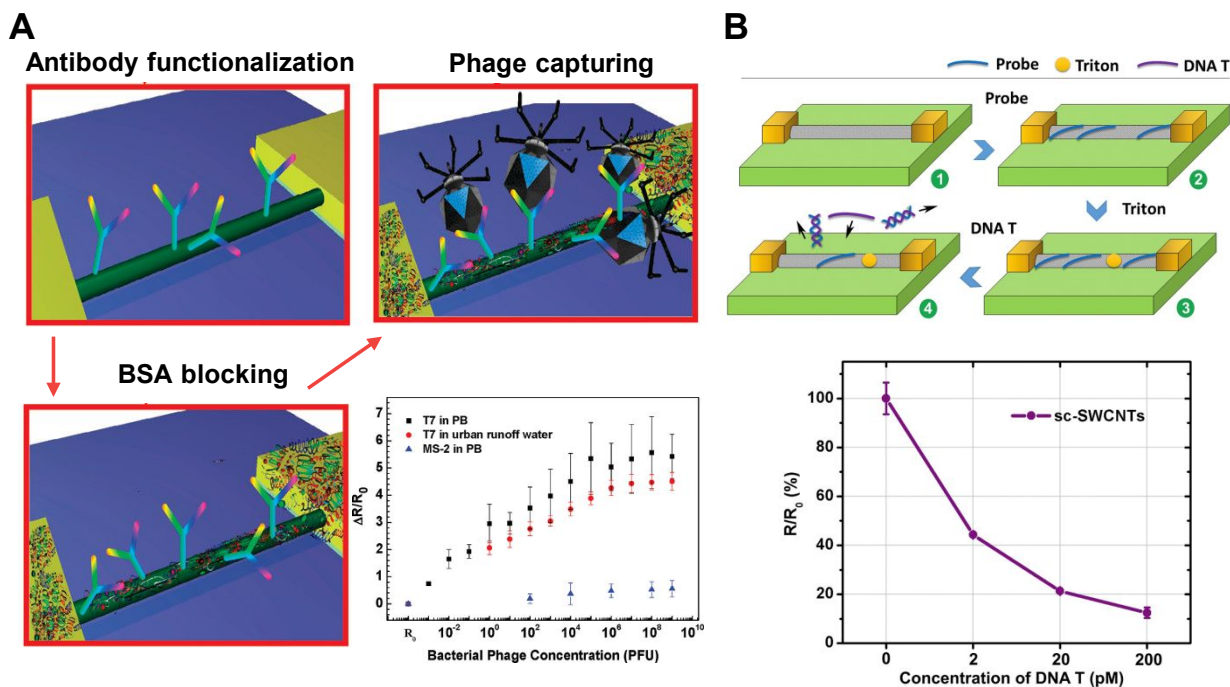


Figure 7. Chemiresistor detection of viruses. (A) Antibody functionalization, BSA blocking, T7 phage capturing, and sensing responses on the sensor surface. The sensor showed high specificity towards T7 phage. Adapted with permission from ref.¹⁶⁶ Copyright 2010 American Chemical

1
2
3 Society. (B) Schematic illustration of CNT-based chemiresistor functionalization and sensing
4 procedures for influenza A virus H5N1 DNA. The increase in DNA concentration caused a
5 decrease in resistant signal. Adapted with permission from ref.¹⁷¹ Copyright 2017 Elsevier B.V.
6
7

8 **3.2.3 Field-effect transistor (FET) based nanosensors**

9

10 FET-based nanosensors are semiconductor devices with three terminals (i.e., source, drain,
11 and gate)¹⁷³ and the electrical carriers flow in the nanoscale semiconductor channel below the gate
12 between the source and drain. When the analytes with charges bind to the gate, the channel's
13 electrical carrier density and current can change due to the electrostatic interaction for biosensing
14 signal transduction. SiNWs, CNTs, and graphene are the most commonly used semiconductor
15 channel nanomaterials due to their high selectivity and sensitivity, real-time response, and label-
16 free detection capabilities.^{174, 175} For optimal detection sensitivity, it requires careful engineering
17 of semiconductor nanomaterials in device geometry, doping density, and surface properties.^{176, 177}
18
19

20 Recognition elements are usually necessary for FETs and viruses can be detected by
21 monitoring the change in FET conductivity following viral binding to recognition elements on the
22 channel. Jin et al. developed anti-EBOV immobilized reduced graphene oxide (rGO)-FETs to
23 detect inactivated EBOV.¹⁷⁸ A shift in the Dirac voltage was measured when EBOV approached
24 and the LOD reached as low as 2.4 pg/mL. The rGO-FETs showed negligible conductance changes
25 for other viruses, indicating high target specificity. Similarly, Seo et al. recently developed
26 graphene-based FETs for SARS-CoV-2 detection (**Figure 8**).¹⁷⁹ The SARS-CoV-2 spike antibody
27 was conjugated onto the graphene sheet via 1-pyrenebutyric acid n-hydroxysuccinimide ester.
28 Graphene-based FETs successfully detected SARS-CoV-2 at a low level of 16 PFU/mL in culture
29 medium and showed great potential for clinical samples (242 copies/mL). Fathi-Hafshejani et al.
30 reported using a FET sensor for sensitive *in vitro* detection of SARS-CoV-2.¹⁸⁰ The sensor was
31 created by functionalizing tungsten diselenide (WSe₂) monolayers with a monoclonal antibody
32 against SARS-CoV-2 spike protein and exhibited a LOD of ~25 fg/ μ L in PBS. Additional
33
34
35
36
37
38
39
40
41
42
43
44
45
46
47
48
49
50
51
52
53
54
55
56
57
58
59
60

1
2
3 applications of antibody immobilized FETs can be found elsewhere.¹⁸¹⁻¹⁸³ Using an antibody-
4 antigen reaction, H3N2 in simulated aerosol can be detected within 1-2 min by SiNW-FETs,
5 extending the system to field applications.¹⁸²
6
7

8
9
10 In addition to antibodies, other recognition elements have also been used in FETs. Uhm et
11 al. developed ultrasensitive SiNW-based FETs for POC detection of H1N1.¹⁸⁴ Cytidine-5'-
12 monophospho-N-acetylneuraminic acid (CMP-NANA) was employed as a probe since it can
13 specifically bind both to the aldehyde self-aligned monolayer on the SiNWs and the hemagglutinin
14 1 domain of hemagglutinin on the surface of H1N1 simultaneously. The threshold voltage shift
15 could reach 112 mV at 1fM hemagglutinin 1 domain, indicating high sensitivity for H1N1.
16
17 Recently, Park et al. developed a dual-gate FET by functionalizing ACE2 to specifically capture
18 SARS-CoV-2.¹⁸⁵ The developed sensor can successfully detect SARS-CoV-2 in 20 min with a
19 LOD of ~165 copies/mL.
20
21
22
23
24
25
26
27
28
29

30
31 In addition to the direct detection of virus particles, nucleic acids have also been used to
32 determine viruses by FETs. The hybridization of probe DNA and the target DNA/RNA can lead
33 to a change in charge density that induces a change in the electric field. The immobilization of the
34 DNA probe can first affect the output signals. Using CNTs-FETs to detect H1N1 DNA, Tran et al.
35 found that if the density of probe DNA was too high, the strongly repulsive electrostatic force
36 among the bases of the DNA strands would make it disadvantageous for the DNA interaction.¹⁸⁶
37
38 By optimizing the experimental conditions, the response time of the DNA sensor was less than
39 one minute and the LOD for H1N1 DNA reached 1 pM. Gao et al. reported an ultrasensitive poly-
40 L-lysine (PLL)-functionalized graphene FET sensor for breast cancer cell miRNAs and SARS-
41 CoV-2 RNA detection.¹⁸⁷ PLL exhibits a high affinity toward graphene and nucleic acids which
42 can enhance the immobilization of DNA probes. The developed sensor-enabled SARS-CoV-2
43
44
45
46
47
48
49
50
51
52
53
54
55
56
57
58
59
60

RNA detection with a LOD of as low as 1 fM within 20 min. To enhance the immobilization of the DNA probe, some metal oxide NWs have been used in FETs. Shariati developed FETs based on indium tin oxide (ITO) NWs.¹⁸⁸ The intensive conductance and functional modified surface of ITO NWs increased DNA probe immobilization and target DNA hybridization. The LOD for hepatitis B virus (HBV) DNA was 1 pM. Also, the developed ITO NWs device allowed label-free discrimination between the fully matched and mismatched DNAs, offering a unique advantage over other technologies which require labeling and additional tags.

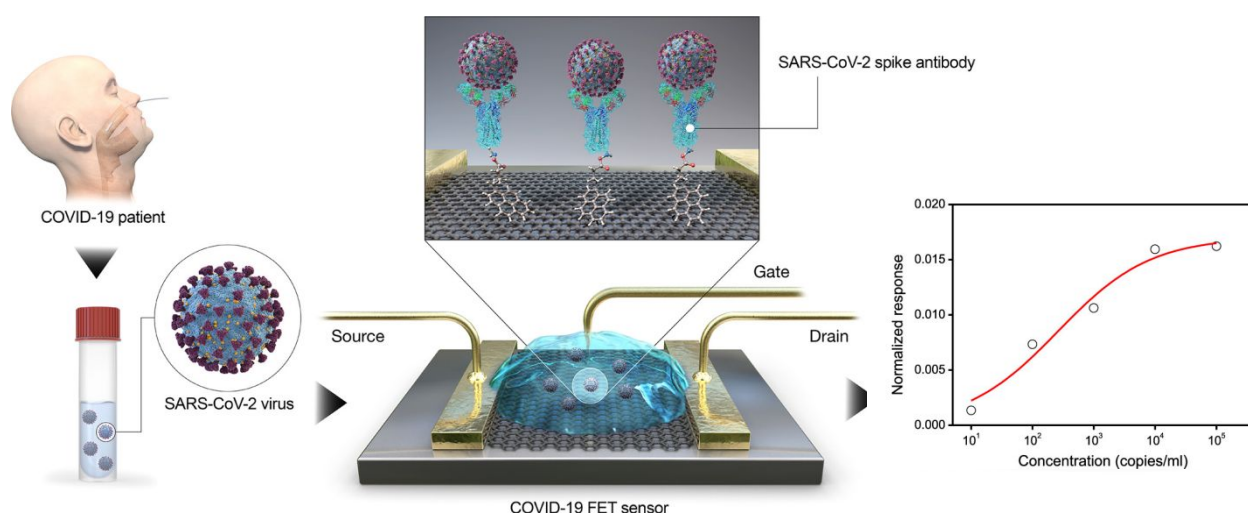


Figure 8. FETs-based nanosensors for SARS-CoV-2 detection through the SARS-CoV-2 spike antibody conjugated graphene sheet. The signal response increase with the concentration of SARS-CoV-2 from clinical samples. Adapted with permission from ref.¹⁷⁹ Copyright 2020 American Chemical Society.

3.3 Magnetic nanosensors

Optical and electrical nanosensors typically use nanomaterials (or modified nanomaterials) as active transducers with high surface sensitivity to convert analyte binding events into optical and electrical readout signals for virus detection. In contrast, magnetic nanosensors typically act as labels, leading to a change in the magnetic signal.¹⁸⁹ The following section is broken into two parts according to the magnetic signal readout device: magnetoresistance and magnetic relaxation switching.

3.3.1 Magnetoresistance (MR) nanosensors

With combined magnetic and electrical properties, MR nanosensors allow the signal transduction process that the electrical resistance can change in response to the binding of magnetic NPs to the sensor surface. Compared with typical optical nanosensors, MR nanosensors exhibit lower background noise and are less affected by environmental factors such as pH and temperature.¹⁹⁰ MR nanosensors can be further classified into anisotropic magnetoresistance (AMR), giant magnetoresistance (GMR), and tunneling magnetoresistance (TMR) nanosensors.¹⁹¹

MR nanosensors for virus detection are generally based on the detection of DNA. As discussed by Su et al.¹⁹¹, most MR nanosensors for detecting DNA can be summarized in the following steps: The DNA probe is first immobilized onto the MR sensor surface. Usually, target DNA is modified with biotin and then attached to the MR sensor surface to hybridize with the DNA probe. Then streptavidin-coated magnetic NPs are added to the MR sensor and captured by the target DNA via the strong non-covalent interaction between biotin and streptavidin. Finally, the MR sensor converts the number of adhered magnetic NPs into electrical signals and DNA is quantified. In this way, Yang et al. developed MR nanosensors for quick and parallel genotyping of human papilloma virus (HPV) type 16/18.¹⁹² Combined with other technologies, GMR nanosensors can reach low LODs for viruses. For example, Zhi et al. successfully detected HBV genotypes by combining GMR nanosensors with LAMP and the LOD is reported to be as low as 10 copies/mL.¹⁹³

Since viral DNA detection requires laborious effort for pretreatment (e.g., DNA extraction), many researchers have turned to directly detecting viral antigen. The mechanism to detect the viral antigen is similar to that for detecting DNA.¹⁹¹ Capture antibody is modified on the surface of the substrate and binds with the virus and biotinylated detection antibodies in succession. Then,

streptavidin-coated magnetic NPs are captured through the biotin-streptavidin reaction. Krishna et al. developed a sensitive detection method for H1N1 based on GMR nanosensors (**Figure 9A**).¹⁹⁴ The capture of magnetic NPs onto the sensors resulted in a resistance change that was measured in real-time by the electrical readout. The sensors could successfully detect H1N1 at levels as low as 150 TCID₅₀/mL. Subsequently, the same group has worked to improve the detection of viruses by GMR nanosensors. They developed a portable GMR handheld platform for POC H1N1 detection (**Figure 9B**).¹⁹⁵ The GMR sensors were embedded in a handheld testing system (Z-Lab) and the real-time change in the magnetoresistance ratio (ΔMR) was monitored for virus quantification. The LOD of this portable Z-lab was 125 TCID₅₀/mL. Furthermore, they optimized their handheld testing system by adapting the wash-free magnetic bioassay, which was more cost-effective for real-time monitoring and showed great potential for daily sensing.¹⁹⁶

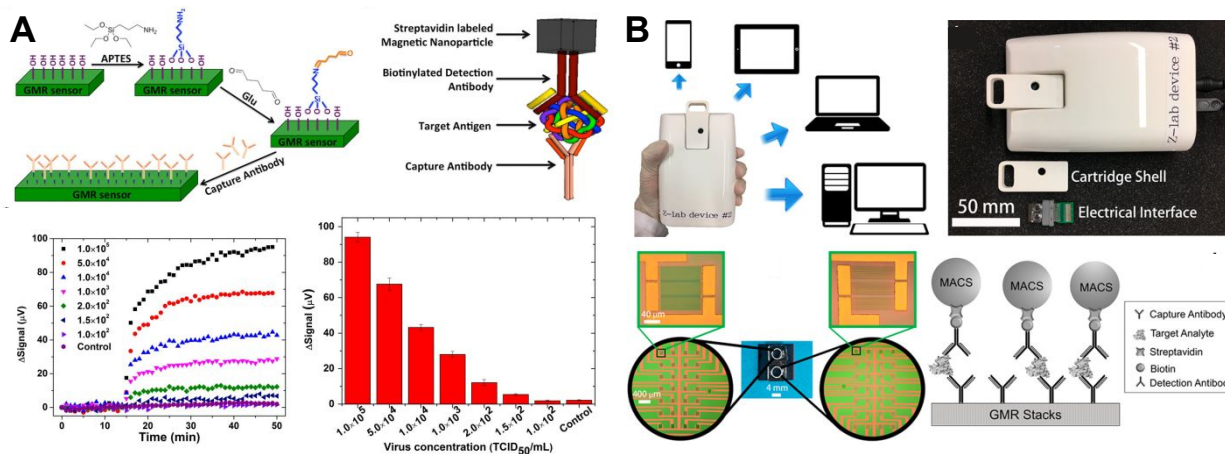


Figure 9. MR-based nanosensors detection of viruses. (A) Detection of influenza A virus through a typical sandwich structure modified with an antibody. The signal increased with concentration and reaction time. Adapted with permission from ref.¹⁹⁴ Copyright 2016 Frontiers. (C) the portable GMR handheld platform for the detection of the influenza A virus. Adapted with permission from ref.¹⁹⁵ Copyright 2017 American Chemical Society.

3.3.2 Magnetic relaxation switching (MRS) nanosensors

MRS nanosensors detect changes in the transverse relaxation time (T_2) of the surrounding water molecules caused by the aggregation or disaggregation of magnetic NPs in the presence of

1
2
3 an analyte.¹⁹⁷ Generally, such changes can be divided into type I (T2 decreases with the aggregation)
4 or type II (T2 increases with the aggregation). These changes can be monitored by common nucleic
5 magnetic resonance (NMR) and magnetic resonance imaging (MRI) instrumentation.
6
7

8
9
10 The behavior of type I and type II based MRS assays for detecting influenza virus
11 hemagglutinin was compared by Koh et al.¹⁹⁸ They found that both type I and type II based MRS
12 assays could successfully detect the Tag peptide of influenza virus hemagglutinin using the
13 monoclonal antibody (anti-Tag) modified magnetic NPs. The type II-based assay showed better
14 sensitivity than the type I-based assay. The specificity and sensitivity of the MRS nanosensors can
15 be enhanced by modifying the magnetic NP signal source. Perez et al. utilized a bifunctional linker,
16 suberic acid bis (N-hydroxysuccinimide ester) to cross-link the amino groups both in the specific
17 antibody and superparamagnetic iron oxide NPs to detect herpes simplex virus (HSV) and AdV in
18 biological media (**Figure 10A**).¹⁹⁹ A very low concentration of viral particles (5 viral particles in
19 10 μ L) can cause a detectable magnetic change (δT_2) through this method.
20
21
22
23
24
25
26
27
28
29
30
31
32

33 To increase the sensitivity of MRS nanosensors and achieve more rapid detection. Chen et
34 al. developed a method based on MRS and magnetic separation to detect Newcastle disease virus
35 (NDV) (**Figure 10B**).²⁰⁰ This method takes advantage of the improved magnetic separation of
36 magnetic beads with a larger size (MB₂₅₀) to capture and enrich target Newcastle disease virus.
37 Smaller magnetic beads (MB₃₀) were chosen as magnetic probes since they could not easily be
38 separated. Following the removal of the MB₂₅₀-virus-MB₃₀ complex, the remaining T2 of MB₃₀
39 was detected and used for quantification of NDV. This approach showed higher sensitivity (10²
40 copy/mL) for NDV than the conventional MRS sensor (10³ copy/mL).
41
42
43
44
45
46
47
48
49
50
51
52
53
54
55
56
57
58
59
60

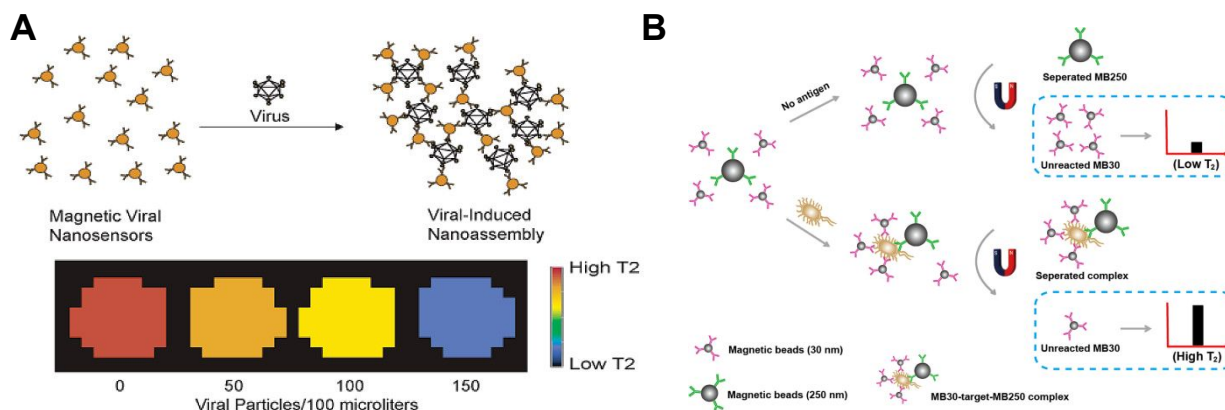


Figure 10. MRS-based nanosensors detection of viruses. (A) The clustering of the antibody-conjugated magnetic NPs in the presence of the virus occurs with a corresponding change in the MR signal (δT_2). Adapted with permission from ref.¹⁹⁹ Copyright 2003 American Chemical Society. (B) The capture and enrichment of the NDV and the T2 signal readout of water molecules around the unreacted MB30. Adapted with permission from ref.²⁰⁰ Copyright 2015 American Chemical Society.

4. Conclusions and future research needs

Understanding virus transmission in the environment and developing rapid and reliable virus detection methods for complicated environmental samples are two pivotal but still unmet needs to address current and future viral outbreaks. Concerted efforts are needed to bridge the disconnect between epidemiological and environmental sciences and enable a proactive and prompt approach to unexpected outbreaks. To date, insufficient knowledge of how viruses spread in many environments makes it difficult to control outbreaks proactively. While highly sensitive, the gold standard PCR-based diagnostics for clinical application suffer from long processing periods and limited supplies.

In this review, we summarized environmental virus transmission routes and then discussed in detail the recent applications of nanosensors for virus detection. Nanosensors can potentially enable rapid response, facile operation, and thus are platforms to advance virus detection more rapidly than conventional approaches. Various nanosensors have been actively developed and

1
2
3 show promise for virus detection with high sensitivity, reliability, and a short detection period.
4
5 Many nanosensors are field-deployable and potentially suitable for mass production. Also, when
6
7 combined with different analytical tools there is the potential to improve nanosensor efficacy.
8
9
10 Micro- or nano-fluidic devices have been successfully incorporated with nanosensors for virus
11
12 detection.^{81, 150} Meanwhile, nanosensors can be easily used for POC/POU virus detection through
13
14 handheld devices.^{90, 195}
15
16

17 Although the development of nanosensors for virus detection is gradually maturing, there
18
19 remain issues that need to be addressed if they are to be commercialized for field applications. For
20
21 instance, while nanosensor sensitivity is readily reported, device and platform stability are much
22
23 less studied. Virus sampling inevitably comes with interference from environmental, food, and
24
25 clinical samples that may deteriorate the accuracy of the detection method. Most of the work
26
27 described in the literature relies upon laboratory settings or is applied to clinical samples. The
28
29 effects of environmental stressors and interferents (e.g., pH, salinity, organic matter) on detection
30
31 accuracy must be investigated and reported. Also, despite many developments in nanosensors,
32
33 most such platforms are currently geared toward medical applications. For successful application
34
35 of nanosensors in environmental samples, we need environment-centered strategies that improve
36
37 different aspects of nanosensors (**Box 1**). Also, future research should be directed to fill the
38
39 knowledge gaps between related fields such as epidemiology, environmental science and
40
41 engineering, and aerosol science. We close with a list of standards that reflect the current status of
42
43 nanosensors for virus detection in the environment and discuss the need for future research (**Box**
44
45
46
47
48
49 **2**).
50
51
52
53
54
55
56
57
58
59
60

Box 1. Linking virus environmental transmission to nanosensors: Potential challenges that need additional research effort.

Despite many successes in the development of nanosensors for virus detection, their application in environmental settings remains underexplored relative to clinical samples. The potential impacts of factors from a range of environments should be demonstrated. We condense such strategies into three priorities to realize the application of nanosensors for the detection of viruses in the environment.

1) Environmental transmission. Although we have highlighted environmental routes of viral dissemination, there remains a need for scientific investigation of transmission routes to appropriately design effective sampling strategies. For example, the relative importance of airborne transmission routes of SARS-CoV-2 has been disputed.²⁰¹ The appropriate detection approach will be highly dependent upon whether SARS-CoV-2 transmits primarily via droplets or aerosols.

2) Environmental media. Environmental composition is dependent upon the specific medium (water, air, food) under consideration. During virus sampling, background constituents will be present along with target viruses and may interfere with nanosensor performance. Accordingly, it is imperative to investigate the potential effects of interferents on the nanosensors. *Water:* Suspended solids, natural organic matter (NOM), and inorganic/organic contaminants are common constituents in water samples. pH may also have an impact on nanosensor stability.¹³ *Food:* Fat and proteins from meat, juice, or milk; cellulose from plant matter; oil and physiological fluids from soils and livestock feces may impact nanosensor performance.²⁰² *Air:* Alkaline species (e.g., ammonia), organic acids (e.g., sulfuric acids) and particulate matter need to be considered. Considering potential inferences from numerous compositions in environmental media, it is important to evaluate the performance of any nanosensor (e.g., LOD) in a range of environments. For example, the real-time RT-PCR and RT-LAMP for detection of SARS-CoV-2 had LODs of 0.41 copies/ μ L and 0.4 copies/ μ L in sewage samples.^{203, 204} Nanosensor sensitivity needs to be evaluated in real environmental media and then the results explicitly compared to conventional approaches under the same conditions.

3) Environmental sampling. The concentration of viruses of interest in environmental samples are often low and thus sampling schemes that are able to concentrate viral loads are an important, yet often poorly considered aspect of effective environmental nanosensor application. Existing approaches for sample concentration include the following. *Water:* samples can be processed by an adsorption-elution method using commercially available filters. *Air:* samples can be collected by a variety of different aerosol samplers. *Food:* samples can be processed using an elution buffer after being cut into small pieces. To date, the recovery rates of such sampling filters and elution buffers have not been explicitly explored nor compared. Establishment of standard methods that report expected recovery rates for different environments remains an important need.

Box 2. Nanosensor criteria for virus detection in environmental samples

Despite the considerable literature on development of nanosensors for virus detection, there remain few reports illustrating their application for environmental sample analysis. Here we summarize the current status of nanosensors for detection of virus in environmental samples and we discuss the need for future research.

Sensitivity and specificity. The sensitivity and specificity of current nanosensors achieved through measurable signal change and specific recognition elements are often reportedly comparable to conventional methods such as RT-PCR and ELISA. (e.g., LODs of nanosensors for SARS-CoV-2 are ~ 80 copies/mL¹⁰³). However, complex environmental interferences and the buffers or chemicals involved in the sample handling process may affect nanosensor stability and performance. Sensitivity and specificity should be evaluated using real environmental samples that contain virus, or at a minimum in samples spiked with virus that use representative matrices. Reported LODs and units should be standardized across the literature for comparison.

Field-deployability and cost. Nanosensors promise device miniaturization and the capacity for multiplex detection with the promised goal of low-cost detection. Considering that samples can be collected from various viral transmission routes at different spatiotemporal scales, the field-deployability and cost of nanosensors are important criteria. Device cost can be reduced through low-cost device fabrication, reductions in sample handling reagents, and through the use of field-deployable read-out device integration. Nanomaterials can be incorporated into paper-based platforms to develop sensor chips or into lateral flow devices.²⁰⁵ For example, a cotton swab stick-based nanosensor manufactured for 15 cents can be used for the detection of SARS-CoV-2.²⁰⁶ Low-cost, handheld readout devices such as cell phones and portable Raman instruments are also available and can be operated by solar or battery power.

Turnaround time Simple and rapid reaction kinetics between the virus and the recognition element of the nanosensor are favorable given the relatively long turnaround times of many conventional methods (e.g., a few hours for PCR-based assays). The output signals following viral recognition can be collected in a short time (e.g., a few seconds¹²² to a few minutes¹⁰³, or even in real-time²⁰⁷). Such rapid turnaround times can minimize sample manipulation and storage. Data visualization with handheld screens can further help achieve rapid turnaround time.

Glossary Table

Abbreviations	Expansions
Viruses	
SARS-CoV	Severe acute respiratory syndrome coronavirus
SARS-CoV-2	Severe acute respiratory syndrome coronavirus 2
MERS-CoV	Middle east respiratory syndrome coronavirus
EBOV	Ebola virus
ZIKV	Zika virus
HAV, HBV, HCV, and HEV	Hepatitis A, B, C and E virus
NoV	Norovirus
AdV	Adenovirus
Ad5	Adenovirus type 5
RV	Rotavirus
CHIKV	Chikungunya virus
DENV	Dengue virus
PCV2	Porcine circovirus type 2
PPV	Porcine parvovirus
PRV	Porcine pseudorabies virus
PVX	Potato virus X
Cv3/CVB3	Coxsackievirus type 3
MYXV	Myxomatosis virus
CDV	Canine distemper virus
CMV	Cucumber mosaic virus
TMV	Tobacco mosaic virus
EMCV	Encephalomyocarditis virus
RSV	Respiratory syncytial virus
EV71	Enterovirus 71
CTV	Citrus tristeza virus
ORSV	Odontoglossum ringspot virus
ALV	Avian leukosis virus
HPV	Human papilloma virus
HSV	Herpes simplex virus
NDV	Newcastle disease virus
Nanomaterials	
NPs	Nanoparticles
NWs	Nanowires
AuNPs and AgNPs	Gold and silver nanoparticles
AuNRs and AgNRs	Gold and silver nanorods
AuNSs	Gold nanostars
AuNZs	Gold nanozymes
Fe ₃ O ₄ NPs	Iron oxide nanoparticles
SiNWs	Silicon nanowires
CNTs	Carbon nanotubes
SWCNTs and MWCNTs	Single-walled and multi-walled carbon nanotubes

1
2
3
4
5
6
7
8
9
10
11
12
13
14
15
16
17
18
19
20
21
22
23
24
25
26
27
28
29
30
31
32
33
34
35
36
37
38
39
40
41
42
43
44
45
46
47
48
49
50
51
52
53
54
55
56
57
58
59
60

AuCNTs	Gold decorated carbon nanotubes
QDs	Quantum dots
RuSi NPs	Ru(bpy) ₃ ²⁺ in silica nanoparticles
CuNCs	Copper nanocomposite
MOFs	Metal-organic frameworks
GO	Graphene oxide
rGO	Reduced graphene oxide
mrGO	Magnetic reduced graphene oxide
V ₂ O ₅	Vanadium oxide
VONP-LPs	V ₂ O ₅ -encapsulated liposomes
TiO ₂	Titanium oxide
ZnO	Zinc oxide
ZnONRs	Zinc oxide nanorods
WSe ₂	Tungsten diselenide
ITO	Indium tin oxide

Technical terminologies

PCR	Polymerase chain reaction
LAMP	Loop-mediated isothermal amplification
ELISA	Enzyme-linked immunosorbent assays
SELEX	Systematic evolution of ligands by exponential enrichment
RT	Reverse transcription/Reverse transcribed
PFU	Plaque-forming unit
TCID ₅₀	50% tissue culture infectious dose
HAU	Hemagglutination unit
POC and POU	Point-of-care and point-of-use
LF	Lateral flow
CL	Control line
TL	Test line
LOD	Limit of detection
LDA	Linear discriminant analysis
RH	Relative humidity
SPR	Surface plasmon resonance
LSPR	Localized surface plasmon resonance
SERS	Surface-enhanced Raman scattering
VERS	Volume-enhanced Raman scattering
EM	Electromagnetic
NIR	Near-infrared
DPV	Differential pulse voltammetry
FRET	Fluorescence resonance electron transfer
PAFI	Plasmonic-assisted fluoroimmunoassay
MagLISA	Magnetic nanozyme-linked immunosorbent assay
MFIA	Magnetofluoroimmunoassay
FICT	Fluorescent immunochromatographic strips test

1		
2		
3	NEA	Nanoelectrode array
4	SAM	Self-assembled monolayer
5	FET	Field-effect transistor
6	EIS	Electrochemical impedance spectroscopy
7	ECL	Electrochemiluminescence
8	MR	Magnetoresistance
9	AMR	Anisotropic magnetoresistance
10	GMR	Giant magnetoresistance
11	TMR	Tunneling magnetoresistance
12	MRS	Magnetic relaxation switching
13	NMR	Nucleic magnetic resonance
14	MRI	Magnetic resonance imaging
15		
16	Chemicals	
17		
18	HRP	Horseradish peroxidase
19	IgG	Immunoglobulin
20	TMB	3',5,5'-tetramethylbenzidine
21	H ₂ O ₂	Hydrogen peroxide
22	PDA	Polydiacetylene
23	ACE2	Angiotensin-converting enzyme 2
24	S protein	Spike glycoprotein
25	GBP	Gold binding peptide
26	RBITC	Rhodamine B isothiocyanate
27	MGITC	Malachite green isothiocyanate
28	OHT	Oseltamivir hexylthiol
29	Cy3	Cyanine 3
30	4-ATP	4-aminothiophenol
31	6-FAM	6-carboxyfluorescent
32	EDC	1-ethyl-3-(3-dimethylaminopropyl) carbodiimide
33	NHS	N-hydroxysuccinimide
34	MB	Methylene blue
35	Ppy	Polypyrrole
36	HSA	Human serum albumin
37	GOD	Glucose oxidase
38	S RBD	Spike protein receptor binding domain
39	PLL	Poly-L-lysine
40	ssDNA	Single-stranded DNA
41	CMP-NANA	Cytidine-5'-monophospho-N-acetylneuraminic acid
42	PBS	Phosphate-buffered saline
43		
44		
45		
46		
47		
48		
49		
50		
51		
52		
53		
54		
55		
56		
57		
58		
59		
60		

Table 1. Summary of nanosensors for the detection of SARS-CoV-2

Method	Recognition element	General approach	LOD	Reference
Optical				
Colorimetric	Antibody	Colloidal AuNPs functionalized with antibodies targeted viral proteins and the extinction spectrum showed red-shifted.	equivalent to the C_t of 36.5 for PCR	78
SERS	ACE2	Au nanoneedles functionalized with ACE2 targeted viral S protein, exhibiting SERS signals of SARS-CoV-2.	80 copies/mL	103
SERS	ACE2	Ag nanorod array functionalized with ACE2 targeted viral S protein, quenching, and shifting the SERS signals of ACE2.	N/A	104
SERS	Aptamer	Au nanopopcorn array functionalized with aptamer targeted viral S protein, releasing the aptamer with the Raman reporter.	<10 PFU/mL	111
Fluorometric	ACE2	SWCNTs functionalized with ACE2 targeted viral S protein, leading to fluorescence increases.	12.6 nM	122
Electrical				
Electrochemical	EDC/NHS	GO-based electrodes functionalized with AuNS and EDC/NHS interacted with viral glycoprotein, leading to a differentiable DPV.	1.68×10^{-22} ug/mL	151
Electrochemical	Aptamer	AuNPs functionalized with ssDNA targeted viral RNA and immobilized on an electrochemical platform, leading to output voltage changes.	6.9 copies/ μ L	161
Electrochemical	Aptamer	Au@Fe ₃ O ₄ functionalized with aptamer targeted viral RNA and captured on rGO-based platform, resulting in high conductivity.	200 copies/mL	162
Electrochemical	Aptamer	SiNPs functionalized with redox dyes and aptamer targeted viral N gene and captured by aptamer functionalized magnetic NPs, resulting in DPV changes.	1 copy/ μ L	163
FET	Antibody	Graphene-based FET functionalized with antibody targeted virus and viral spike protein, inducing electrical signal changes.	16 PFU/ml, 242 copies/ml	179
FET	Antibody	WSe ₂ based FET functionalized with antibody through 11-MUA targeted virus and viral spike protein, inducing electrical signal changes.	25 fg/ μ L	180
FET	ACE2	A dual-gate FET functionalized ACE2 captured virus and the voltage shift was analyzed at the reference current.	165 copies/mL	185
FET	Aptamer	PLL is functionalized on surface of graphene-FET to immobilize DNA probes. The electrical signals were measured when applying for viral RNA detection.	1 fM	187

Table 2. Summary of nanosensors for the detection of influenza virus

Method	Virus type	Recognition element	General approach	LOD	Reference
Optical					
Colorimetric	H1N1, H3N2	Antibody	Au and Fe ₃ O ₄ NPs functionalized with antibody captured the virus and separated by a magnet. AuNPs catalyzed TMB oxidation and turned the aqueous solution color to blue in positive samples	4.42x10 ⁻¹⁴ g/mL (H1N1), 2.5 PFU/mL (H3N2)	83
Colorimetric	H3N2	Antibody	Au-CNTs functionalized with antibody captured the virus. Au-CNTs catalyzed TMB oxidation and turned the aqueous solution color to blue in positive samples	3.4 PFU/mL	84
Colorimetric	H1N1	Peptide	PDA NPs functionalized with peptide captured the virus and it perturbed the backbone of PDA, resulting in the aqueous solution color change from blue to red.	10 ⁵ PFU	87
SERS	H1N1	N/A	A high-density tip-to-tip Au concave-shape nanostructured substrate captured the virus	10 ⁴ PFU/mL	102
SERS	H1N1	Antibody	Au NPs functionalized with antibody and the Raman reporter formed the sandwich structure with the capture substrate in the presence of virus	4.1×10 ³ TCID/mL	106
SERS	H1N1	Antibody	Au NPs functionalized with antibody and the Raman reporter formed the sandwich structure with the capture substrate in the presence of virus	6 TCID ₅₀ /mL	107
SERS	H1N1	OHT	Au NPs functionalized with OHT formed the sandwich with the capture substrate in the presence of oseltamivir-resistant virus	1 PFU	110
SERS	H3N2	Aptamer	Aptamer with the Raman reporter formed the sandwich with the AgNP coated capture substrate in the presence of virus	10 ⁻⁴ HAU	113
SERS	H7N9	Antibody	Au@Ag NPs functionalized with the antibody and the Raman reporter was captured on the TL of the LFIA strip in the presence of virus	0.0018 HAU	115
SERS	H1N1	Antibody	Ag@Fe ₃ O ₄ NPs functionalized with the antibody and the Raman reporter enriched the virus from impurities by a magnet and was captured on the TL of the LFIA strip.	50 PFU/mL	117
Fluorometric	H1N1	Antibody	AuNPs and QDs functionalized with the antibody captured the virus and exhibited LSPR-induced fluorescence enhancement in positive samples	0.03 pg/mL (water); 0.4 pg/mL (human serum)	125
Fluorometric	H1N1, H3N2	Antibody	AuNP decorated CNTs and QDs functionalized with the antibody captured the virus and exhibited LSPR-induced fluorescence enhancement in positive samples	0.1 pg/mL (water); 50 PFU/mL (clinical sample)	126

1						
2						
3						
4	Fluorometric	H1N1	Antibody	AuNPs and QDs were connected through the peptide chain that was functionalized with antibody. Virus attachment to the peptide chain led to the fluorescence quenching in positive samples.	17.02 fg/mL	128
5						
6	Fluorometric	H1N1	Antibody	Fluorescent NPs conjugated with the virus were captured on the TL in FICT. The TL/CL ratio was used for quantification.	<20 HAU/mL	131
7						
8	Fluorometric	H7N1, H7N9	Antibody	Fluorescent NPs conjugated with the virus were captured on the TL in FICT. The TL/CL ratio was used for quantification.	40 HAU/mL	133
9						
10	Fluorometric	H5N1	Aptamer	The aptamer captured the virus and QD fluorescence reporter was released from the quencher.	0.4 HAU	134
11						
12						
13	Electrical					
14	Electrochemical	H1N1	N/A	AgNPs were adsorbed on a carbon electrode in the presence of H1N1 and current spikes were quantified.	sub pM level	146
15						
16	Electrochemical	H1N1, H5N1, H7N9	Antibody	ZnONR functionalized with antibody targeted virus. HRP-conjugated detection antibody was captured by virus and oxidized TMB in sensing region, resulting in current changes.	1 pg/mL	150
17						
18	Electrochemical	H9N2	Antibody	RuSi NPs and magnetic NPs functionalized with antibody captured virus on an Au modified ITO electrode, enhancing ECL signals.	14 fg/mL	157
19						
20	Chemiresistor	H5N1	Aptamer	CNTs functionalized with DNA probe sequence captured viral DNA, leading to the resistance changes.	2pM	171
21						
22	FET	H3N2	Antibody	SiNWs functionalized with antibody captured virus, resulting in discrete nanowire conductance changes.	10 ⁴ viruses/L	182
23						
24	FET	H1N1	CMP- NANA	SiNWs functionalized with CMP-NANA through the aldehyde self-aligned monolayer bound to hemagglutinin 1, causing voltage shifts.	1pM	184
25						
26	FET	H1N1	Aptamer	CNT-FET immobilized with probe DNA hybridized with target DNA. The charge transfer between DNA and CNT led to a decrease of the drain current.	1pM	186
27						
28						
29						
30						
31	Magnetic					
32	MR	H1N1	Antibody	Streptavidin-coated magnetic NPs with antibody captured on sensors in the presence of virus, resulting in a resistance change.	150 TCID ₅₀ /mL	194
33						
34	MR	H3N2	Antibody	Streptavidin-coated magnetic NPs with antibody captured on a portable GMR platform the presence of virus. The magnetoresistance ratio was measured.	125 TCID ₅₀ /mL	195
35						
36	MR	H1N1, H3N2	Antibody	The target virus-detection antibody- magnetic NPs complex was captured by antibody, gave rise to the positive signals	250 TCID ₅₀ /mL	196
37						
38	MRS	N/A	Antibody	Magnetic NPs functionalized with anti-Tag captured target, resulting in changes in the spin-spin relaxation time.	N/A	198
39						
40						
41						
42						
43						
44						
45						
46						
47						

Table 3. Summary of nanosensors for the detection of other viruses

Method	Virus type	Recognition element	General approach	LOD	Reference
Optical					
Colorimetric	EV71	Antibody	Liposome functionalized with antibody was retrieved in the presence of the virus. The liposome lysis released multiple enzymes that disassembled AuNP aggregates, resulting in a color change from blue to red.	16 copies/ μ L	80
Colorimetric	ZIKV, CHIKV	Aptamer	AuNPs functionalized with aptamer formed sandwich with the capture substrate in the presence of the virus. Ag reagent addition on the AuNP surface caused color change.	1 pM (PBS); 100 pM (calf blood)	81
Colorimetric	DENV	Aptamer	Au and γ -Fe ₂ O ₃ NPs functionalized with aptamer targeted the virus, leading to color change.	N/A	82
Colorimetric	NoV-LPs	Antibody	Graphene-AuNPs functionalized with antibody captured the virus. AuNPs catalyzed TMB oxidation and turned the aqueous solution color to blue in positive samples.	92.7 pg/mL	85
Colorimetric	NoV-LPs	Antibody	Fe ₂ O ₃ and V ₂ O ₅ NPs functionalized with antibody captured the virus. AuNPs catalyzed TMB oxidation and turned the aqueous solution color to blue in positive samples.	0.34 pg/mL	86
Colorimetric	RV	Antibody	Au nanopillars functionalized with antibody captured the virus, leading to LSPR peak shift.	126 PFU/mL	89
SERS	PCV2, PPV, PRV	N/A	Porous carbon film coated AgNPs captured the virus	10 ⁷ copies/mL	98
SERS	PVX	Antibody	AuNRs functionalized with aptamer and the Raman reporter formed the sandwich with the Au shell magnetic NPs in the presence of the virus	2.2 ng/mL	99
SERS	Ad5, Cv3	N/A	Hollow Au nanocones with the opening size for virus loading captured the virus in the vicinity of the SERS hot-spots	N/A	100
SERS	MYXV, CDV, TMV, PVX	N/A	The pore-like Au nano-cavities captured the virus in the vicinity of the SERS hot-spots	N/A	101
SERS	AdV, EMCV	N/A	A high-density tip-to-tip Au concave-shape nanostructured substrate captured the virus in the vicinity of the SERS hot-spots	10 ⁶ PFU/mL	102

1						
2						
3						
4	SERS	PRV	Antibody	AuAg@Ag NPs functionalized with the antibody and the Raman reporter was captured on the TL of the LFIA trip in the presence of virus	5 ng/mL	116
5						
6	SERS	AdV	Antibody	Ag@Fe ₃ O ₄ NPs functionalized with the antibody and the Raman reporter enriched the virus from impurities by a magnet and was captured on the TL of the LFIA trip.	10 PFU/mL	117
7						
8						
9	SERS	RSV	Antibody	HRP conjugated antibody in the sandwich complex converted TMB to positive, bound to negatively charged AgNPs	0.05 pg/mL	118
10						
11	Fluorometric	CTV	Antibody	Free CTV replaced protein conjugated AuNPs to bind with antibody-conjugated QDs and increased fluorescent signal	0.13 μg/mL	124
12						
13					1716	
14	Fluorometric	EV71, CVB3	Antibody	Magnetic nanobeads and QDs functionalized with antibody captured the viruses and exhibited fluorescence signal in positive samples after magnetic separation.	copies/mL (EV71);1618 copies/mL (CVB3)	129
15						
16						
17						
18	Fluorometric	NoV	Antibody	Au/magnetic NPs and QD functionalized with antibody captured the virus and exhibited LSPR-induced fluorescence enhancement in positive samples.	0.48 pg/mL	130
19						
20						
21						
22	Fluorometric	NoV	Aptamer	Quenched fluorescence was recovered after the release of the 6-FAM labeled aptamer in the presence of the virus	4.4 and 3.3 ng/mL with MWCNTs and GO	121
23						
24						
25	Electrical					
26						
27	Electrochemical	Vaccinia virus	N/A	Carbon nanofiber NEA was able to capture virus and led to impedance changes between NEA and an ITO electrode.	~2.58 × 10 ³ particles/mL	145
28						
29	Electrochemical	ORSV	Antibody	Micro/nano hybrid-structured Au electrodes functionalized with SAM and antibodies targeted virus, leading to EIS responses.	0.238 ng/mL	148
30						
31	Electrochemical	NoV	Peptide and aptamer	Magnetic nanocomposites modified with aptamer captured by peptide modified electrode in the presence of virus, leading to current change.	0.8 copy/mL	152
32						
33	Electrochemical	NoV	Peptide	WS ₂ NF/AuNP were modified by peptides to capture virus and caused the impedance change.	2.37 copies/mL	153
34						
35						
36	Electrochemical	ALV	Antibody	Fe ₃ O ₄ NPs functionalized with antibody and GOD captured by antibody and β-cyclodextrin-ferrocene functionalized GO platform in the presence of virus, leading to DPV changes.	10 ^{2.19} TCID ₅₀ /mL	156
37						
38						
39	Electrochemical	HCV	Aptamer	CuNPs were synthesized and introduced to rGO when target DNA bound with probe DNA. The electrochemical signal of the oxidation of o-phenylenediamine were recorded in the presence CuNPs.	405 pM	158
40						
41						
42						
43						
44						
45						
46						
47						

1						
2						
3						
4	Electrochemical	DENV	Aptamer	ZnO/Pt-Pd modified electrode were functionalized with probe DNA. The electrochemical response of the intercalation of MB and dsDNA were determined.	4.3×10^{-5} M	159
5						
6						
7	Electrochemical	Agrovirus	Aptamer	MWCNTs-CuNPs coated on electrode were functionalized with probe DNA. DPV were determined when viral DNA bound with probe DNA on to reduce MB.	0.01 ng/ μ L	160
8						
9						
10	Electrochemical	ZIKV	Antibody	Au array-based electrode functionalized with antibody targeted ZIKV protein, leading to EIS changes.	10pM	164
11						
12	Chemiresistor	T7, MS2	Antibody	Ppy NWs functionalized with antibodies targeted viruses, leading to NWs resistance changes.	10^{-3} PFU	166
13						
14	Chemiresistor	CMV	Antibody	Ppy nanoribbons functionalized with antibody targeted virus, leading to electrical resistance changes.	10 ng/mL	167
15						
16	Chemiresistor	DENV	Heparin	SWCNT on electrode was functionalized with heparin. The resistance changed when heparin bound with virus.	8.4×10^2 TCID ₅₀ /mL	169
17						
18	FET	EBOV	Antibody	rGO modified FET was functionalized with antibody to target virus. The response was measured by the shift of Dirac voltage.	2.4 pg/mL	178
19						
20	FET	EBOV	Antibody	FET was modified with rGO, Al ₂ O ₃ and AuNPs and functionalized with antibody. The electronic-resonance frequency was measured.	1 ng/mL	181
21						
22	FET	EBOV	Antibody	FET was modified with rGO, Al ₂ O ₃ and AuNPs and functionalized with antibody. The electronic-resonance frequency was measured.	0.001 mg/L	183
23						
24	FET	HBV	Aptamer	ITO NWs functionalized with DNA probe targeted viral DNA, leading to a change in drain current.	1pM	188
25						
26						
27	Magnetic					
28	MR	HPV	Aptamer	Streptavidin-coated magnetic NPs were captured by biotin modified target DNA. The changes giant magnetoimpedance were detected.	N/A	192
29						
30	MR	HBV	Aptamer	Streptavidin-coated magnetic NCs were captured by biotin modified target DNA. Magnetic signal was measured	10 copies/mL	193
31						
32	MRS	HSV, AdV	Antibody	Virus induced antibody functionalized magnetic NPs assembly and resulted in spin-spin relaxation time changes	5 viral particles in 10 μ L	199
33						
34	MRS	NDV	Antibody	Larger magnetic NPs were used to capture virus while smaller magnetic NPs acted as magnetic probes	100 copies/mL	200
35						
36						
37						
38						
39						
40						
41						
42						
43						
44						
45						
46						
47						

Reference

1. P. A. Rota, M. S. Oberste, S. S. Monroe, W. A. Nix, R. Campagnoli, J. P. Icenogle, S. Penaranda, B. Bankamp, K. Maher and M.-h. Chen, Characterization of a novel coronavirus associated with severe acute respiratory syndrome, *Science*, 2003, **300**, 1394-1399.
2. D. J. Jamieson, M. A. Honein, S. A. Rasmussen, J. L. Williams, D. L. Swerdlow, M. S. Biggerstaff, S. Lindstrom, J. K. Louie, C. M. Christ and S. R. Bohm, H1N1 2009 influenza virus infection during pregnancy in the USA, *Lancet*, 2009, **374**, 451-458.
3. S. K. Gire, A. Goba, K. G. Andersen, R. S. Sealfon, D. J. Park, L. Kanneh, S. Jalloh, M. Momoh, M. Fullah and G. Dudas, Genomic surveillance elucidates Ebola virus origin and transmission during the 2014 outbreak, *Science*, 2014, **345**, 1369-1372.
4. I. K. Oboho, S. M. Tomczyk, A. M. Al-Asmari, A. A. Banjar, H. Al-Mugti, M. S. Aloraini, K. Z. Alkhalidi, E. L. Almohammadi, B. M. Alraddadi and S. I. Gerber, 2014 MERS-CoV outbreak in Jeddah—a link to health care facilities, *New Engl. J. Med.*, 2015, **372**, 846-854.
5. G. S. Campos, A. C. Bandeira and S. I. Sardi, Zika virus outbreak, bahia, brazil, *Emerg. Infect. Dis.*, 2015, **21**, 1885.
6. World Health Organization (WHO). Coronavirus disease 2019 (COVID-19): situation report. Available at: <https://www.who.int/emergencies/diseases/novel-coronavirus-2019/situation-reports>. Accessed June, 2022.
7. I. Kong, Y. Park, Y. Woo, J. Lee, J. Cha, J. Choi, Y. Kim, J. Kim, S. Park and M. Yum, Early epidemiological and clinical characteristics of 28 cases of coronavirus disease in South Korea, *Osong Public Health Res. Perspect.*, 2020, **11**, 8-14.
8. B. Adelodun, F. O. Ajibade, A. O. Tiamiyu, N. A. Nwogwu, R. G. Ibrahim, P. Kumar, V. Kumar, G. Odey, K. K. Yadav and A. H. Khan, Monitoring the presence and persistence of SARS-CoV-2 in water-food-environmental compartments: State of the knowledge and research needs, *Environ. Res.*, 2021, **200**, 111373.
9. World Health Organization (WHO). Modes of transmission of virus causing COVID-19: implications for IPC precaution recommendations: scientific brief, 27 March, 2020.
10. B. Roche and P. Rohani, Environmental transmission scrambles coexistence patterns of avian influenza viruses, *Epidemics*, 2010, **2**, 92-98.
11. R. Gonzalez, K. Curtis, A. Bivins, K. Bibby, M. H. Weir, K. Yetka, H. Thompson, D. Keeling, J. Mitchell and D. Gonzalez, COVID-19 surveillance in Southeastern Virginia using wastewater-based epidemiology, *Water Res.*, 2020, **186**, 116296.
12. P. J. Vikesland and K. R. Wigginton, Nanomaterial Enabled Biosensors for Pathogen Monitoring - A Review, *Environ. Sci. Technol.*, 2010, **44**, 3656-3669.
13. P. J. Vikesland, Nanosensors for water quality monitoring, *Nat. Nanotechnol.*, 2018, **13**, 651-660.
14. D. Rodriguez-Lazaro, N. Cook, F. M. Ruggeri, J. Sellwood, A. Nasser, M. S. J. Nascimento, M. D'Agostino, R. Santos, J. C. Saiz and A. Rzeżutka, Virus hazards from food, water and other contaminated environments, *FEMS Microbiol. Rev.*, 2012, **36**, 786-814.
15. M. Elsamadony, M. Fujii, T. Miura and T. Watanabe, Possible transmission of viruses from contaminated human feces and sewage: Implications for SARS-CoV-2, *Sci. Total Environ.*, 2021, **755**, 142575.
16. B. J. Cowling, D. K. Ip, V. J. Fang, P. Suntarattiwong, S. J. Olsen, J. Levy, T. M. Uyeki, G. M. Leung, J. M. Peiris and T. Chotpitayasunondh, Aerosol transmission is an important mode of influenza A virus spread, *Nat. Commun.*, 2013, **4**, 1935.
17. Z. Altintas, M. Gittens, J. Pocock and I. E. Tothill, Biosensors for waterborne viruses: Detection and removal, *Biochimie*, 2015, **115**, 144-154.
18. I. Xagorarakis, Z. Yin and Z. Svambayev, Fate of viruses in water systems, *J. Environ. Eng.*, 2014, **140**, 04014020.

19. M. V. A. Corpuz, A. Buonerba, G. Vigliotta, T. Zarra, F. Ballesteros Jr, P. Campiglia, V. Belgiorno, G. Korshin and V. Naddeo, Viruses in wastewater: occurrence, abundance and detection methods, *Sci. Total Environ.*, 2020, **745**, 140910.
20. W. Ahmed, B. Tschärke, P. M. Bertsch, K. Bibby, A. Bivins, P. Choi, L. Clarke, J. Dwyer, J. Edson and T. M. H. Nguyen, SARS-CoV-2 RNA monitoring in wastewater as a potential early warning system for COVID-19 transmission in the community: A temporal case study, *Sci. Total Environ.*, 2021, **761**, 144216.
21. S. P. Sherchan, S. Shahin, L. M. Ward, S. Tandukar, T. G. Aw, B. Schmitz, W. Ahmed and M. Kitajima, First detection of SARS-CoV-2 RNA in wastewater in North America: A study in Louisiana, USA, *Sci. Total Environ.*, 2020, **743**, 140621.
22. E. Haramoto, B. Malla, O. Thakali and M. Kitajima, First environmental surveillance for the presence of SARS-CoV-2 RNA in wastewater and river water in Japan, *Sci. Total Environ.*, 2020, **737**, 140405.
23. W. Ahmed, N. Angel, J. Edson, K. Bibby, A. Bivins, J. W. O'Brien, P. M. Choi, M. Kitajima, S. L. Simpson and J. Li, First confirmed detection of SARS-CoV-2 in untreated wastewater in Australia: A proof of concept for the wastewater surveillance of COVID-19 in the community, *Sci. Total Environ.*, 2020, **728**, 138764.
24. C. J. Campos, J. Avant, J. Lowther, D. Till and D. N. Lees, Human norovirus in untreated sewage and effluents from primary, secondary and tertiary treatment processes, *Water Res.*, 2016, **103**, 224-232.
25. X. Pang, Y. Qiu, T. Gao, R. Zurawell, N. F. Neumann, S. Craik and B. E. Lee, Prevalence, levels and seasonal variations of human enteric viruses in six major rivers in Alberta, Canada, *Water Res.*, 2019, **153**, 349-356.
26. H. Lee, M. Kim, J. E. Lee, M. Lim, M. Kim, J. M. Kim, W. H. Jheong, J. Kim and G. Ko, Investigation of norovirus occurrence in groundwater in metropolitan Seoul, Korea, *Sci. Total Environ.*, 2011, **409**, 2078-2084.
27. T. Miura, A. Gima and M. Akiba, Detection of norovirus and rotavirus present in suspended and dissolved forms in drinking water sources, *Food Environ. Virol.*, 2019, **11**, 9-19.
28. H. Wang, I. Kjellberg, P. Sikora, H. Rydberg, M. Lindh, O. Bergstedt and H. Norder, Hepatitis E virus genotype 3 strains and a plethora of other viruses detected in raw and still in tap water, *Water Res.*, 2020, **168**, 115141.
29. C. P. Gerba and W. Q. Betancourt, Assessing the Occurrence of Waterborne Viruses in Reuse Systems: Analytical Limits and Needs, *Pathogens*, 2019, **8**, 107.
30. R. Leiva-Rebollo, A. M. Labella, E. J. Valverde, D. Castro and J. J. Borrego, Persistence of Lymphocystis Disease Virus (LCDV) in Seawater, *Food Environ. Virol.*, 2020, **12**, 174-179.
31. P. Khare and L. Marr, Simulation of vertical concentration gradient of influenza viruses in dust resuspended by walking, *Indoor Air*, 2015, **25**, 428-440.
32. C. C. Wang, K. A. Prather, J. Sznitman, J. L. Jimenez, S. S. Lakdawala, Z. Tufekci and L. C. Marr, Airborne transmission of respiratory viruses, *Science*, 2021, **373**, eabd9149.
33. L. Morawska and J. Cao, Airborne transmission of SARS-CoV-2: The world should face the reality, *Environ. Int.*, 2020, **139**, 105730.
34. M. D. Christian, M. Loutfy, C. McDonald, K. F. Martinez, M. Ofner, T. Wong, T. Wallington, W. L. Gold, B. Mederski, K. Green, D. E. Low and S. I. Team, Possible SARS coronavirus transmission during cardiopulmonary resuscitation, *Emerg. Infect. Dis.*, 2004, **10**, 287-293.
35. C. Zemouri, S. Awad, C. Volgenant, W. Crielaard, A. Laheij and J. De Soet, Modeling of the transmission of coronaviruses, measles virus, influenza virus, Mycobacterium tuberculosis, and Legionella pneumophila in dental clinics, *J. Dent. Res.*, 2020, **99**, 1192-1198.
36. X. Zhao, W. Nie, C. Zhou, M. Cheng, C. Wang, Y. Liu, J. Li, Y. Qian, X. Ma and L. Zhang, Airborne Transmission of Influenza Virus in a Hospital of Qinhuangdao During 2017–2018 Flu Season, *Food Environ. Virol.*, 2019, **11**, 427-439.

- 1
- 2
- 3 37. Y. Liu, Z. Ning, Y. Chen, M. Guo, Y. Liu, N. K. Gali, L. Sun, Y. Duan, J. Cai, D. Westerdahl, X.
- 4 Liu, K. Xu, K.-f. Ho, H. Kan, Q. Fu and K. Lan, Aerodynamic analysis of SARS-CoV-2 in two
- 5 Wuhan hospitals, *Nature*, 2020, **582**, 557-560.
- 6 38. C. Xie, E. H. Lau, T. Yoshida, H. Yu, X. Wang, H. Wu, J. Wei, B. Cowling, M. Peiris and Y. Li,
- 7 Detection of influenza and other respiratory viruses in air sampled from a university campus: a
- 8 longitudinal study, *Clin. Infect. Dis.*, 2020, **70**, 850-858.
- 9 39. K. K. Coleman and W. V. Sigler, Airborne Influenza A Virus Exposure in an Elementary School,
- 10 *Sci. Rep.*, 2020, **10**, 1859.
- 11 40. K. Lin and L. C. Marr, Humidity-Dependent Decay of Viruses, but Not Bacteria, in Aerosols and
- 12 Droplets Follows Disinfection Kinetics, *Environ. Sci. Technol.*, 2019, **54**, 1024-1032.
- 13 41. J. Tamerius, S. Ojeda, C. K. Uejio, J. Shaman, B. Lopez, N. Sanchez and A. Gordon, Influenza
- 14 transmission during extreme indoor conditions in a low-resource tropical setting, *Int. J.*
- 15 *Biometeorol.*, 2017, **61**, 613-622.
- 16 42. P. Wolkoff, Indoor air humidity, air quality, and health—An overview, *Int. J. Hyg. Environ. Health*,
- 17 2018, **221**, 376-390.
- 18 43. A. Bosch, R. M. Pintó and S. Guix, Foodborne viruses, *Curr. Opin. Food Sci.*, 2016, **8**, 110-119.
- 19 44. R. C. Miranda and D. W. Schaffner, Virus risk in the food supply chain, *Curr. Opin. Food Sci.*,
- 20 2019, **30**, 43-48.
- 21 45. A. Bosch, E. Gkogka, F. S. Le Guyader, F. Loisy-Hamon, A. Lee, L. van Lieshout, B. Marthi, M.
- 22 Myrmet, A. Sansom, A. C. Schultz, A. Winkler, S. Zuber and T. Phister, Foodborne viruses:
- 23 Detection, risk assessment, and control options in food processing, *Int. J. Food Microbiol.*, 2018,
- 24 **285**, 110-128.
- 25 46. P. Liu, M. Yang, X. Zhao, Y. Guo, L. Wang, J. Zhang, W. Lei, W. Han, F. Jiang and W. J. Liu,
- 26 Cold-chain transportation in the frozen food industry may have caused a recurrence of COVID-19
- 27 cases in destination: successful isolation of SARS-CoV-2 virus from the imported frozen cod
- 28 package surface, *Biosafety and health*, 2020, **2**, 199-201.
- 29 47. J. Brassard, M.-J. Gagné, M. Génereux and C. Côté, Detection of human food-borne and zoonotic
- 30 viruses on irrigated, field-grown strawberries, *Appl. Environ. Microbiol.*, 2012, **78**, 3763-3766.
- 31 48. H. Shin, H. Park, D. J. Seo, S. Jung, D. Yeo, Z. Wang, K. H. Park and C. Choi, Foodborne Viruses
- 32 Detected Sporadically in the Fresh Produce and Its Production Environment in South Korea,
- 33 *Foodborne Pathog. Dis.*, 2019, **16**, 411-420.
- 34 49. Y. Somura, M. Nagano, K. Kimoto, M. Oda, K. Mori, T. Shinkai and K. Sadamasu, Detection of
- 35 norovirus in food samples collected during suspected food - handler - involved foodborne
- 36 outbreaks in Tokyo, *Lett. Appl. Microbiol.*, 2019, **69**, 175-180.
- 37 50. Y. Lu, M. M. Ma, H. Wang, D. H. Wang, C. Chen, Q. L. Jing, J. M. Geng, T. G. Li, Z. B. Zhang
- 38 and Z. C. Yang, An outbreak of norovirus-related acute gastroenteritis associated with delivery
- 39 food in Guangzhou, southern China, *BMC Public Health*, 2020, **20**, 25.
- 40 51. J. Han, X. Zhang, S. He and P. Jia, Can the coronavirus disease be transmitted from food? A review
- 41 of evidence, risks, policies and knowledge gaps, *Environ. Chem. Lett.*, 2020, **19**, 5-16.
- 42 52. K. L. Burkhalter and H. M. Savage, Detection of Zika virus in desiccated mosquitoes by real-time
- 43 reverse transcription PCR and plaque assay, *Emerg. Infect. Dis.*, 2017, **23**, 680-681.
- 44 53. S. Pfefferle, S. Reucher, D. Nörz and M. Lütgehetmann, Evaluation of a quantitative RT-PCR assay
- 45 for the detection of the emerging coronavirus SARS-CoV-2 using a high throughput system,
- 46 *Eurosurveillance*, 2020, **25**, 2000152.
- 47 54. R. Lu, X. Wu, Z. Wan, Y. Li, X. Jin and C. Zhang, A Novel Reverse Transcription Loop-Mediated
- 48 Isothermal Amplification Method for Rapid Detection of SARS-CoV-2, *Int. J. Mol. Sci.*, 2020, **21**,
- 49 2826.
- 50 55. F. J. DeGraves, D. Gao and B. Kaltenboeck, High-sensitivity quantitative PCR platform,
- 51 *BioTechniques*, 2003, **34**, 106-115.
- 52 56. C. Uribe-Alvarez, Q. Lam, D. A. Baldwin and J. Chernoff, Low saliva pH can yield false positives
- 53 results in simple RT-LAMP-based SARS-CoV-2 diagnostic tests, *PLoS one*, 2021, **16**, e0250202.
- 54
- 55
- 56
- 57
- 58
- 59
- 60

- 1
2
3 57. P. Hardinge and J. A. Murray, Reduced false positives and improved reporting of loop-mediated
4 isothermal amplification using quenched fluorescent primers, *Sci. Rep.*, 2019, **9**, 7400.
- 5 58. M. N. Aoki, B. de Oliveira Coelho, L. G. B. Góes, P. Minoprio, E. L. Durigon, L. G. Morello, F.
6 K. Marchini, I. N. Riediger, M. do Carmo Debur, H. I. Nakaya and L. Blanes, Colorimetric RT-
7 LAMP SARS-CoV-2 diagnostic sensitivity relies on color interpretation and viral load, *Sci. Rep.*,
8 2021, **11**, 9026.
- 9 59. X. Wang, H. Yao, X. Xu, P. Zhang, M. Zhang, J. Shao, Y. Xiao and H. Wang, Limits of detection
10 of 6 approved RT-PCR kits for the novel SARS-Coronavirus-2 (SARS-CoV-2), *Clin. Chem.*, 2020,
11 **66**, 977-979.
- 12 60. Y. He, T. Xie and Y. Tong, Rapid and highly sensitive one-tube colorimetric RT-LAMP assay for
13 visual detection of SARS-CoV-2 RNA, *Biosens. Bioelectron.*, 2021, **187**, 113330.
- 14 61. V. Roy, S. Fischinger, C. Atyeo, M. Slein, C. Loos, A. Balazs, C. Luedemann, M. G. Astudillo, D.
15 Yang and D. R. Wesemann, SARS-CoV-2-specific ELISA development, *J. Immunol. Methods*,
16 2020, **484**, 112832.
- 17 62. S. Hosseini, P. Vázquez-Villegas, M. Rito-Palomares and S. O. Martinez-Chapa, in *Enzyme-Linked*
18 *Immunoassay (ELISA)*, Springer, 2018, pp. 67-115.
- 19 63. D. K. Gramotnev and S. I. Bozhevolnyi, Plasmonics beyond the diffraction limit, *Nat. Photonics*,
20 2010, **4**, 83-91.
- 21 64. J. A. Schuller, E. S. Barnard, W. Cai, Y. C. Jun, J. S. White and M. L. Brongersma, Plasmonics for
22 extreme light concentration and manipulation, *Nat. Mater.*, 2010, **9**, 193-204.
- 23 65. L. G. Bousiakou, H. Gebavi, L. Mikac, S. Karapetis and M. Ivanda, Surface Enhanced Raman
24 Spectroscopy for Molecular Identification-a Review on Surface Plasmon Resonance (SPR) and
25 Localised Surface Plasmon Resonance (LSPR) in Optical Nanobiosensing, *Croat. Chem. Acta*,
26 2019, **92**, 479-494.
- 27 66. R. Deng, H. Qu, L. Liang, J. Zhang, B. Zhang, D. Huang, S. Xu, C. Liang and W. Xu, Tracing the
28 therapeutic process of targeted aptamer/drug conjugate on cancer cells by surface-enhanced Raman
29 scattering spectroscopy, *Anal. Chem.*, 2017, **89**, 2844-2851.
- 30 67. T.-D. Li, R. Zhang, H. Chen, Z.-P. Huang, X. Ye, H. Wang, A.-M. Deng and J.-L. Kong, An
31 ultrasensitive polydopamine bi-functionalized SERS immunoassay for exosome-based diagnosis
32 and classification of pancreatic cancer, *Chem. Sci.*, 2018, **9**, 5372-5382.
- 33 68. J. Chen, Y. Huang, P. Kannan, L. Zhang, Z. Lin, J. Zhang, T. Chen and L. Guo, Flexible and
34 adhesive surface enhance Raman scattering active tape for rapid detection of pesticide residues in
35 fruits and vegetables, *Anal. Chem.*, 2016, **88**, 2149-2155.
- 36 69. R. Peng, Y. Si, T. Deng, J. Zheng, J. Li, R. Yang and W. Tan, A novel SERS nanoprobe for the
37 ratiometric imaging of hydrogen peroxide in living cells, *Chem. Commun.*, 2016, **52**, 8553-8556.
- 38 70. H. Wei, M. R. Willner, L. C. Marr and P. J. Vikesland, Highly stable SERS pH nanoprobe
39 produced by co-solvent controlled AuNP aggregation, *Analyst*, 2016, **141**, 5159-5169.
- 40 71. S. Ghaderi, B. Ramesh and A. M. Seifalian, Fluorescence nanoparticles “quantum dots” as drug
41 delivery system and their toxicity: a review, *J. Drug Targeting*, 2011, **19**, 475-486.
- 42 72. U. Resch-Genger, M. Grabolle, S. Cavaliere-Jaricot, R. Nitschke and T. Nann, Quantum dots
43 versus organic dyes as fluorescent labels, *Nat. Methods*, 2008, **5**, 763-775.
- 44 73. M. Haase and H. Schäfer, Upconverting nanoparticles, *Angew. Chem. Int. Ed.*, 2011, **50**, 5808-
45 5829.
- 46 74. A. Karami, M. Hasani, F. A. Jalilian and R. Ezati, Conventional PCR Assisted Single-Component
47 Assembly of Spherical Nucleic Acids for Simple Colorimetric Detection of SARS-CoV-2, *Sens.*
48 *Actuators B: Chem.*, 2020, **328**, 128971.
- 49 75. B. Udugama, P. Kadhiresan, H. N. Kozłowski, A. Malekjahani, M. Osborne, V. Y. Li, H. Chen, S.
50 Mubareka, J. B. Gubbay and W. C. Chan, Diagnosing COVID-19: the disease and tools for
51 detection, *ACS Nano*, 2020, **14**, 3822-3835.
- 52 76. S. Talebian, G. G. Wallace, A. Schroeder, F. Stellacci and J. Conde, Nanotechnology-based
53 disinfectants and sensors for SARS-CoV-2, *Nat. Nanotechnol.*, 2020, **15**, 618-621.
- 54
55
56
57
58
59
60

- 1
2
3 77. B. Sepúlveda, P. C. Angelomé, L. M. Lechuga and L. M. Liz-Marzán, LSPR-based nanobiosensors, *Nano today*, 2009, **4**, 244-251.
- 4
5 78. B. D. Ventura, M. Cennamo, A. Minopoli, R. Campanile, S. B. Censi, D. Terracciano, G. Portella
6 and R. Velotta, Colorimetric test for fast detection of SARS-CoV-2 in nasal and throat swabs, *ACS*
7 *Sens.*, 2020, **5**, 3043-3048.
- 8
9 79. S. Diegoli, A. L. Manciulea, S. Begum, I. P. Jones, J. R. Lead and J. A. Preece, Interaction between
10 manufactured gold nanoparticles and naturally occurring organic macromolecules, *Sci. Total*
11 *Environ.*, 2008, **402**, 51-61.
- 12
13 80. L.-H. Xiong, S. Huang, Y. Huang, F. Yin, F. Yang, Q. Zhang, J. Cheng, R. Zhang and X. He,
14 Ultrasensitive Visualization of Virus via Explosive Catalysis of an Enzyme Muster Triggering Gold
15 Nano-aggregate Disassembly, *ACS Appl. Mater. Interfaces*, 2020, **12**, 12525-12532.
- 16
17 81. N. Saraf, M. Villegas, B. J. Willenberg and S. Seal, Multiplex Viral Detection Platform Based on
18 a Aptamers-Integrated Microfluidic Channel, *ACS omega*, 2019, **4**, 2234-2240.
- 19
20 82. C. R. Basso, B. P. Crulhas, M. Magro, F. Vianello and V. A. Pedrosa, A new immunoassay of
21 hybrid nanomater conjugated to aptamers for the detection of dengue virus, *Talanta*, 2019, **197**,
22 482-490.
- 23
24 83. S. Oh, J. Kim, V. T. Tran, D. K. Lee, S. R. Ahmed, J. C. Hong, J. Lee, E. Y. Park and J. Lee,
25 Magnetic nanozyme-linked immunosorbent assay for ultrasensitive influenza A virus detection,
26 *ACS Appl. Mater. Interfaces*, 2018, **10**, 12534-12543.
- 27
28 84. S. R. Ahmed, J. Kim, T. Suzuki, J. Lee and E. Y. Park, Enhanced catalytic activity of gold
29 nanoparticle-carbon nanotube hybrids for influenza virus detection, *Biosens. Bioelectron.*, 2016,
30 **85**, 503-508.
- 31
32 85. S. R. Ahmed, K. Takemura, T.-C. Li, N. Kitamoto, T. Tanaka, T. Suzuki and E. Y. Park, Size-
33 controlled preparation of peroxidase-like graphene-gold nanoparticle hybrids for the visible
34 detection of norovirus-like particles, *Biosens. Bioelectron.*, 2017, **87**, 558-565.
- 35
36 86. A. B. Ganganboina, A. D. Chowdhury, I. M. Khoris, F. Nasrin, K. Takemura, T. Hara, F. Abe, T.
37 Suzuki and E. Y. Park, Dual modality sensor using liposome-based signal amplification technique
38 for ultrasensitive norovirus detection, *Biosens. Bioelectron.*, 2020, **157**, 112169.
- 39
40 87. S. Song, K. Ha, K. Guk, S.-G. Hwang, J. M. Choi, T. Kang, P. Bae, J. Jung and E.-K. Lim,
41 Colorimetric detection of influenza A (H1N1) virus by a peptide-functionalized polydiacetylene
42 (PEP-PDA) nanosensor, *RSC adv.*, 2016, **6**, 48566-48570.
- 43
44 88. J.-p. Jeong, E. Cho, D. Yun, T. Kim, I.-S. Lee and S. Jung, Label-free colorimetric detection of
45 influenza antigen based on an antibody-polydiacetylene conjugate and its coated polyvinylidene
46 difluoride membrane, *Polymers*, 2017, **9**, 127.
- 47
48 89. M. Rippa, R. Castagna, S. Brandi, G. Fusco, M. Monini, D. Chen, J. Zhou, J. Zyss and L. Petti,
49 Octupolar Plasmonic Nanosensor Based on Ordered Arrays of Triangular Au Nanopillars for
50 Selective Rotavirus Detection, *ACS Appl. Nano Mater.*, 2020, **3**, 4837-4844.
- 51
52 90. Z. Rong, Q. Wang, N. Sun, X. Jia, K. Wang, R. Xiao and S. Wang, Smartphone-based fluorescent
53 lateral flow immunoassay platform for highly sensitive point-of-care detection of Zika virus
54 nonstructural protein 1, *Anal. Chim. Acta*, 2019, **1055**, 140-147.
- 55
56 91. J. Z. Zhang, *Optical properties and spectroscopy of nanomaterials*, World Scientific, 2009.
- 57
58 92. M. Fleischmann, P. J. Hendra and A. J. McQuillan, Raman spectra of pyridine adsorbed at a silver
59 electrode, *Chem. Phys. Lett.*, 1974, **26**, 163-166.
- 60
93. D. L. Jeanmaire and R. P. Van Duyne, Surface Raman spectroelectrochemistry: Part I. Heterocyclic,
aromatic, and aliphatic amines adsorbed on the anodized silver electrode, *J. Electroanal. Chem.*
Interf. Electrochem., 1977, **84**, 1-20.
94. R. A. Halvorson and P. J. Vikesland, Surface-Enhanced Raman Spectroscopy (SERS) for
Environmental Analyses, *Environ. Sci. Technol.*, 2010, **44**, 7749-7755.
95. J. Liu and Y. Lu, Preparation of aptamer-linked gold nanoparticle purple aggregates for
colorimetric sensing of analytes, *Nat. Protoc.*, 2006, **1**, 246-252.

- 1
2
3 96. J. Cao, T. Sun and K. T. Grattan, Gold nanorod-based localized surface plasmon resonance
4 biosensors: A review, *Sens. Actuators B: Chem.*, 2014, **195**, 332-351.
- 5 97. L. E. Kreno, N. G. Greeneltch, O. K. Farha, J. T. Hupp and R. P. Van Duyne, SERS of molecules
6 that do not adsorb on Ag surfaces: a metal–organic framework-based functionalization strategy,
7 *Analyst*, 2014, **139**, 4073-4080.
- 8 98. Z. Luo, L. Chen, C. Liang, Q. Wei, Y. Chen and J. Wang, Porous carbon films decorated with silver
9 nanoparticles as a sensitive SERS substrate, and their application to virus identification, *Microchim.*
10 *Acta*, 2017, **184**, 3505-3511.
- 11 99. M. G. Caglayan, E. Kasap, D. Cetin, Z. Suludere and U. Tamer, Fabrication of SERS active gold
12 nanorods using benzalkonium chloride, and their application to an immunoassay for potato virus
13 X, *Microchim. Acta*, 2017, **184**, 1059-1067.
- 14 100. X. Zhang, X. Zhang, C. Luo, Z. Liu, Y. Chen, S. Dong, C. Jiang, S. Yang, F. Wang and X. Xiao,
15 Volume - Enhanced Raman Scattering Detection of Viruses, *Small*, 2019, **15**, 1805516.
- 16 101. N. N. Durmanov, R. R. Guliev, A. V. Eremenko, I. A. Boginskaya, I. A. Ryzhikov, E. A. Trifonova,
17 E. V. Putlyayev, A. N. Mukhin, S. L. Kalnov and M. V. Balandina, Non-labeled selective virus
18 detection with novel SERS-active porous silver nanofilms fabricated by Electron Beam Physical
19 Vapor Deposition, *Sens. Actuators B: Chem.*, 2018, **257**, 37-47.
- 20 102. C.-W. Chang, J.-D. Liao, A.-L. Shiao and C.-K. Yao, Non-labeled virus detection using inverted
21 triangular Au nano-cavities arrayed as SERS-active substrate, *Sens. Actuators B: Chem.*, 2011, **156**,
22 471-478.
- 23 103. Y. Yang, Y. Peng, C. Lin, L. Long, J. Hu, J. He, H. Zeng, Z. Huang, Z.-Y. Li, M. Tanemura, J. Shi,
24 J. R. Lombardi and X. Luo, Human ACE2-Functionalized Gold “Virus-Trap” Nanostructures for
25 Accurate Capture of SARS-CoV-2 and Single-Virus SERS Detection, *Nano-Micro Lett.*, 2021, **13**,
26 109.
- 27 104. D. Zhang, X. Zhang, R. Ma, S. Deng, X. Wang, X. Wang, X. Zhang, X. Huang, Y. Liu, G. Li, J.
28 Qu, Y. Zhu and J. Li, Ultra-fast and onsite interrogation of Severe Acute Respiratory Syndrome
29 Coronavirus 2 (SARS-CoV-2) in waters via surface enhanced Raman scattering (SERS), *Water*
30 *Res.*, 2021, **200**, 117243.
- 31 105. Z. k. Farka, T. s. Juřík, D. Kovář, L. e. Trnková and P. Skládal, Nanoparticle-based
32 immunochemical biosensors and assays: recent advances and challenges, *Chem. Rev.*, 2017, **117**,
33 9973-10042.
- 34 106. J. Moon, S. Y. Yi, A. Hwang, G. Eom, J. Sim, J. Jeong, E.-K. Lim, B. H. Chung, B. Kim, J. Jung
35 and T. Kang, Facile and sensitive detection of influenza viruses using SERS antibody probes, *RSC*
36 *adv.*, 2016, **6**, 84415-84419.
- 37 107. K. Karn-Orachai, K. Sakamoto, R. Laocharoensuk, S. Bamrungsap, S. Songsivilai, T. Dharakul
38 and K. Miki, Extrinsic surface-enhanced Raman scattering detection of influenza A virus enhanced
39 by two-dimensional gold@ silver core–shell nanoparticle arrays, *RSC adv.*, 2016, **6**, 97791-97799.
- 40 108. G. Eom, A. Hwang, D. K. Lee, K. Guk, J. Moon, J. Jeong, J. Jung, B. Kim, E.-K. Lim and T. Kang,
41 Superb Specific, Ultrasensitive, and Rapid Identification of the Oseltamivir-Resistant H1N1 Virus:
42 Naked-Eye and SERS Dual-Mode Assay Using Functional Gold Nanoparticles, *ACS Appl. Bio*
43 *Mater.*, 2019, **2**, 1233-1240.
- 44 109. S. G. Hwang, K. Ha, K. Guk, D. K. Lee, G. Eom, S. Song, T. Kang, H. Park, J. Jung and E.-K.
45 Lim, Rapid and simple detection of Tamiflu-resistant influenza virus: Development of oseltamivir
46 derivative-based lateral flow biosensor for point-of-care (POC) diagnostics, *Sci. Rep.*, 2018, **8**,
47 12999.
- 48 110. G. Eom, A. Hwang, H. Kim, S. Yang, D. K. Lee, S. Song, K. Ha, J. Jeong, J. Jung, E.-K. Lim and
49 T. Kang, Diagnosis of Tamiflu-Resistant Influenza Virus in Human Nasal Fluid and Saliva Using
50 Surface-Enhanced Raman Scattering, *ACS Sens.*, 2019, **4**, 2282-2287.
- 51 111. H. Chen, S.-G. Park, N. Choi, H.-J. Kwon, T. Kang, M.-K. Lee and J. Choo, Sensitive Detection
52 of SARS-CoV-2 Using a SERS-Based Aptasensor, *ACS Sens.*, 2021, **6**, 2378-2385.
- 53
54
55
56
57
58
59
60

- 1
2
3 112. I. Shiratori, J. Akitomi, D. A. Boltz, K. Horii, M. Furuichi and I. Waga, Selection of DNA aptamers
4 that bind to influenza A viruses with high affinity and broad subtype specificity, *Biochem. Biophys.*
5 *Res. Commun.*, 2014, **443**, 37-41.
- 6 113. V. I. Kukushkin, N. M. Ivanov, A. A. Novoseltseva, A. S. Gambaryan, I. V. Yaminsky, A. M.
7 Kopylov and E. G. Zavyalova, Highly sensitive detection of influenza virus with SERS aptasensor,
8 *PLoS one*, 2019, **14**, e0216247.
- 9 114. X. Fu, Z. Cheng, J. Yu, P. Choo, L. Chen and J. Choo, A SERS-based lateral flow assay biosensor
10 for highly sensitive detection of HIV-1 DNA, *Biosens. Bioelectron.*, 2016, **78**, 530-537.
- 11 115. M. Xiao, K. Xie, X. Dong, L. Wang, C. Huang, F. Xu, W. Xiao, M. Jin, B. Huang and Y. Tang,
12 Ultrasensitive detection of avian influenza A (H7N9) virus using surface-enhanced Raman
13 scattering-based lateral flow immunoassay strips, *Anal. Chim. Acta*, 2019, **1053**, 139-147.
- 14 116. H. Shen, K. Xie, L. Huang, L. Wang, J. Ye, M. Xiao, L. Ma, A. Jia and Y. Tang, A novel SERS-
15 based lateral flow assay for differential diagnosis of wild-type pseudorabies virus and gE-deleted
16 vaccine, *Sens. Actuators B: Chem.*, 2019, **282**, 152-157.
- 17 117. C. Wang, C. Wang, X. Wang, K. Wang, Y. Zhu, Z. Rong, W. Wang, R. Xiao and S. Wang,
18 Magnetic SERS strip for sensitive and simultaneous detection of respiratory viruses, *ACS Appl.*
19 *Mater. Interfaces*, 2019, **11**, 19495-19505.
- 20 118. L. Zhan, S. J. Zhen, X. Y. Wan, P. F. Gao and C. Z. Huang, A sensitive surface-enhanced Raman
21 scattering enzyme-catalyzed immunoassay of respiratory syncytial virus, *Talanta*, 2016, **148**, 308-
22 312.
- 23 119. D. Paria, K. S. Kwok, P. Raj, P. Zheng, D. H. Gracias and I. Barman, Label-free spectroscopic
24 SARS-CoV-2 detection on versatile nanoimprinted substrates, *Nano Lett.*, 2022, **22**, 3620-3627.
- 25 120. J. P. Broughton, X. Deng, G. Yu, C. L. Fasching, V. Servellita, J. Singh, X. Miao, J. A. Streithorst,
26 A. Granados, A. Sotomayor-Gonzalez, K. Zorn, A. Gopez, E. Hsu, W. Gu, S. Miller, C.-Y. Pan, H.
27 Guevara, D. A. Wadford, J. S. Chen and C. Y. Chiu, CRISPR-Cas12-based detection of SARS-
28 CoV-2, *Nat. Biotechnol.*, 2020, **38**, 870-874.
- 29 121. X. Weng and S. Neethirajan, Aptamer-based fluorometric determination of norovirus using a paper-
30 based microfluidic device, *Microchim. Acta*, 2017, **184**, 4545-4552.
- 31 122. R. L. Pinals, F. Ledesma, D. Yang, N. Navarro, S. Jeong, J. E. Pak, L. Kuo, Y.-C. Chuang, Y.-W.
32 Cheng, H.-Y. Sun and M. P. Landry, Rapid SARS-CoV-2 spike protein detection by carbon
33 nanotube-based near-infrared nanosensors, *Nano Lett.*, 2021, **21**, 2272-2280.
- 34 123. Y. Cao, T. Xie, R. C. Qian and Y. T. Long, Plasmon resonance energy transfer: coupling between
35 chromophore molecules and metallic nanoparticles, *Small*, 2017, **13**, 1601955.
- 36 124. T. R. Shojaei, M. A. M. Salleh, K. Sijam, R. A. Rahim, A. Mohsenifar, R. Safarnejad and M.
37 Tabatabaei, Detection of Citrus tristeza virus by using fluorescence resonance energy transfer-
38 based biosensor, *Spectrochim. Acta A Mol. Biomol. Spectrosc.*, 2016, **169**, 216-222.
- 39 125. K. Takemura, O. Adegoke, N. Takahashi, T. Kato, T.-C. Li, N. Kitamoto, T. Tanaka, T. Suzuki
40 and E. Y. Park, Versatility of a localized surface plasmon resonance-based gold nanoparticle-
41 alloyed quantum dot nanobiosensor for immunofluorescence detection of viruses, *Biosens.*
42 *Bioelectron.*, 2017, **89**, 998-1005.
- 43 126. J. Lee, S. R. Ahmed, S. Oh, J. Kim, T. Suzuki, K. Parmar, S. S. Park, J. Lee and E. Y. Park, A
44 plasmon-assisted fluoro-immunoassay using gold nanoparticle-decorated carbon nanotubes for
45 monitoring the influenza virus, *Biosens. Bioelectron.*, 2015, **64**, 311-317.
- 46 127. S. Link and M. A. El-Sayed, Size and temperature dependence of the plasmon absorption of
47 colloidal gold nanoparticles, *J. Phys. Chem. B*, 1999, **103**, 4212-4217.
- 48 128. F. Nasrin, A. D. Chowdhury, K. Takemura, I. Kozaki, H. Honda, O. Adegoke and E. Y. Park,
49 Fluorometric virus detection platform using quantum dots-gold nanocomposites optimizing the
50 linker length variation, *Anal. Chim. Acta*, 2020, **1109**, 148-157.
- 51 129. J.-J. Wang, Y.-Z. Jiang, Y. Lin, L. Wen, C. Lv, Z.-L. Zhang, G. Chen and D.-W. Pang,
52 Simultaneous point-of-care detection of enterovirus 71 and coxsackievirus B3, *Anal. Chem.*, 2015,
53 **87**, 11105-11112.
- 54
55
56
57
58
59
60

- 1
2
3 130. K. Takemura, J. Lee, T. Suzuki, T. Hara, F. Abe and E. Y. Park, Ultrasensitive detection of
4 norovirus using a magnetofluoroimmunoassay based on synergic properties of gold/magnetic
5 nanoparticle hybrid nanocomposites and quantum dots, *Sens. Actuators B: Chem.*, 2019, **296**,
6 126672.
- 7 131. S.-T. Yu, C. T. Bui, D. T. H. Kim, A. V. Nguyen, T. T. T. Trinh and S.-J. Yeo, Clinical evaluation
8 of rapid fluorescent diagnostic immunochromatographic test for influenza A virus (H1N1), *Sci.*
9 *Rep.*, 2018, **8**, 13468.
- 10 132. A. V. T. Nguyen, T. D. Dao, T. T. T. Trinh, D.-Y. Choi, S.-T. Yu, H. Park and S.-J. Yeo, Sensitive
11 detection of influenza a virus based on a CdSe/CdS/ZnS quantum dot-linked rapid fluorescent
12 immunochromatographic test, *Biosens. Bioelectron.*, 2020, **155**, 112090.
- 13 133. S.-J. Yeo, D. T. Bao, G.-E. Seo, C. T. Bui, D. T. H. Kim, N. T. V. Anh, T. T. T. Tien, N. T. P. Linh,
14 H.-J. Sohn, C.-K. Chong, H.-J. Shin and H. Park, Improvement of a rapid diagnostic application of
15 monoclonal antibodies against avian influenza H7 subtype virus using Europium nanoparticles, *Sci.*
16 *Rep.*, 2017, **7**, 7933.
- 17 134. L. Xu, R. Wang, L. C. Kelso, Y. Ying and Y. Li, A target-responsive and size-dependent hydrogel
18 aptasensor embedded with QD fluorescent reporters for rapid detection of avian influenza virus
19 H5N1, *Sens. Actuators B: Chem.*, 2016, **234**, 98-108.
- 20 135. X. Kou, S. Jiang, S.-J. Park and L.-Y. Meng, A review: recent advances in preparations and
21 applications of heteroatom-doped carbon quantum dots, *Dalton Trans.*, 2020, **49**, 6915-6938.
- 22 136. Z. Huang, G. Zhai, Z. Zhang, C. Zhang, Y. Xia, L. Lian, X. Fu, D. Zhang and J. Zhang, Low cost
23 and large scale synthesis of PbS quantum dots with hybrid surface passivation, *CrystEngComm*,
24 2017, **19**, 946-951.
- 25 137. S. Shen, J. Wang, Z. Wu, Z. Du, Z. Tang and J. Yang, Graphene quantum dots with high yield and
26 high quality synthesized from low cost precursor of aphanitic graphite, *Nanomaterials*, 2020, **10**,
27 375.
- 28 138. Y. Chen, S. Li, L. Huang and D. Pan, Low-cost and gram-scale synthesis of water-soluble Cu–In–
29 S/ZnS core/shell quantum dots in an electric pressure cooker, *Nanoscale*, 2014, **6**, 1295-1298.
- 30 139. Z. Meng, R. M. Stolz, L. Mendecki and K. A. Mirica, Electrically-transduced chemical sensors
31 based on two-dimensional nanomaterials, *Chem. Rev.*, 2019, **119**, 478-598.
- 32 140. K. Khalid, X. F. Tan, H. F. M. Zaid, Y. Tao, C. L. Chew, D. T. Chu, M. K. Lam, Y. C. Ho, J. W.
33 Lim and L. C. Wei, Advanced in developmental organic and inorganic nanomaterial: a review,
34 *Bioengineered*, 2020, **11**, 328-355.
- 35 141. G. T. Chandran, X. W. Li, A. Ogata and R. M. Penner, Electrically Transduced Sensors Based on
36 Nanomaterials (2012-2016), *Anal. Chem.*, 2017, **89**, 249-275.
- 37 142. T. Ozer, B. J. Geiss and C. S. Henry, Chemical and biological sensors for viral detection, *J.*
38 *Electrochem. Soc.*, 2019, **167**, 037523.
- 39 143. F. R. Baptista, S. A. Belhout, S. Giordani and S. J. Quinn, Recent developments in carbon
40 nanomaterial sensors, *Chem. Soc. Rev.*, 2015, **44**, 4433-4453.
- 41 144. J. M. George, A. Antony and B. Mathew, Metal oxide nanoparticles in electrochemical sensing and
42 biosensing: a review, *Microchim. Acta*, 2018, **185**, 358.
- 43 145. F. R. Madiyar, S. L. Haller, O. Farooq, S. Rothenburg, C. Culbertson and J. Li, Ac dielectrophoretic
44 manipulation and electroporation of vaccinia virus using carbon nanoelectrode arrays,
45 *Electrophoresis*, 2017, **38**, 1515-1525.
- 46 146. L. Sepunaru, B. J. Plowman, S. V. Sokolov, N. P. Young and R. G. Compton, Rapid
47 electrochemical detection of single influenza viruses tagged with silver nanoparticles, *Chem. Sci.*,
48 2016, **7**, 3892-3899.
- 49 147. B. Piro and S. Reisberg, Recent Advances in Electrochemical Immunosensors, *Sensors*, 2017, **17**,
50 794.
- 51 148. W.-J. Wang, C.-H. Lee, C.-W. Li, S. Liao, F.-J. Jan and G.-J. Wang, Orchid Virus Detection from
52 Orchid Leaves Using Micro/Nano Hybrid-Structured Immuno-Electrochemical Biosensor, *J.*
53 *Electrochem. Soc.*, 2020, **167**, 027530.
- 54
55
56
57
58
59
60

- 1
2
3 149. A. Sharma, A. Kaushal and S. Kulshrestha, A Nano-Au/C-MWCNT based label free amperometric
4 immunosensor for the detection of capsicum chlorosis virus in bell pepper, *Arch. Virol.*, 2017, **162**,
5 2047-2052.
- 6 150. J.-H. Han, D. Lee, C. H. C. Chew, T. Kim and J. J. Pak, A multi-virus detectable microfluidic
7 electrochemical immunosensor for simultaneous detection of H1N1, H5N1, and H7N9 virus using
8 ZnO nanorods for sensitivity enhancement, *Sens. Actuators B: Chem.*, 2016, **228**, 36-42.
- 9 151. S. A. Hashemi, N. G. G. Behbahan, S. Bahrani, S. M. Mousavi, A. Gholami, S. Ramakrishna, M.
10 Firoozsani, M. Moghadami, K. B. Lankarani and N. Omidifar, Ultra-sensitive viral glycoprotein
11 detection NanoSystem toward accurate tracing SARS-CoV-2 in biological/non-biological media,
12 *Biosens. Bioelectron.*, 2021, **171**, 112731.
- 13 152. H. Zhao, W. Xie, R.-L. Zhang, X.-D. Wang, H.-F. Liu, J. Li, T. Sha, X.-S. Guo, Q.-M. Sun and Y.-
14 P. Zhang, Electrochemical sensor for human norovirus based on covalent organic
15 framework/pillararene heterosupramolecular nanocomposites, *Talanta*, 2022, **237**, 122896.
- 16 153. S. H. Baek, C. Y. Park, T. P. Nguyen, M. W. Kim, J. P. Park, C. Choi, S. Y. Kim, S. K. Kailasa
17 and T. J. Park, Novel peptides functionalized gold nanoparticles decorated tungsten disulfide
18 nanoflowers as the electrochemical sensing platforms for the norovirus in an oyster, *Food Control*,
19 2020, **114**, 107225.
- 20 154. M. Backer, C. Koch, S. Eiben, F. Geiger, F. Eber, H. Gliemann, A. Poghossian, C. Wege and M. J.
21 Schoning, Tobacco mosaic virus as enzyme nanocarrier for electrochemical biosensors, *Sens.*
22 *Actuators B: Chem.*, 2017, **238**, 716-722.
- 23 155. H. Ilkhani and S. Farhad, A novel electrochemical DNA biosensor for Ebola virus detection, *Anal.*
24 *Biochem.*, 2018, **557**, 151-155.
- 25 156. K. Shang, X. D. Wang, B. Sun, Z. G. Cheng and S. Y. Ai, beta-cyclodextrin-ferrocene host-guest
26 complex multifunctional labeling triple amplification strategy for electrochemical immunoassay of
27 subgroup J of avian leukosis viruses, *Biosens. Bioelectron.*, 2013, **45**, 40-45.
- 28 157. F. Luo, C. Long, Z. Wu, H. Xiong, M. Chen, X. Zhang, W. Wen and S. Wang, Functional silica
29 nanospheres for sensitive detection of H9N2 avian influenza virus based on immunomagnetic
30 separation, *Sens. Actuators B: Chem.*, 2020, **310**, 127831.
- 31 158. J. Li, Y. Li, X. Zhai, Y. Cao, J. Zhao, Y. Tang and K. Han, Sensitive electrochemical detection of
32 hepatitis C virus subtype based on nucleotides assisted magnetic reduced graphene oxide-copper
33 nano-composite, *Electrochem. Commun.*, 2020, **110**, 106601.
- 34 159. C. Singhal, C. Pundir and J. Narang, A genosensor for detection of consensus DNA sequence of
35 Dengue virus using ZnO/Pt-Pd nanocomposites, *Biosens. Bioelectron.*, 2017, **97**, 75-82.
- 36 160. M. A. Tahir, S. Z. Bajwa, S. Mansoor, R. W. Briddon, W. S. Khan, B. E. Scheffler and I. Amin,
37 Evaluation of carbon nanotube based copper nanoparticle composite for the efficient detection of
38 agroviruses, *J. Hazard. Mater.*, 2018, **346**, 27-35.
- 39 161. M. Alafeef, K. Dighe, P. Moitra and D. Pan, Rapid, Ultrasensitive, and Quantitative Detection of
40 SARS-CoV-2 Using Antisense Oligonucleotides Directed Electrochemical Biosensor Chip, *ACS*
41 *Nano*, 2020, **14**, 17028-17045.
- 42 162. H. Zhao, F. Liu, W. Xie, T.-C. Zhou, J. OuYang, L. Jin, H. Li, C.-Y. Zhao, L. Zhang and J. Wei,
43 Ultrasensitive supersandwich-type electrochemical sensor for SARS-CoV-2 from the infected
44 COVID-19 patients using a smartphone, *Sens. Actuators B: Chem.*, 2021, **327**, 128899.
- 45 163. T. Chaibun, J. Puenpa, T. Ngamdee, N. Boonapatcharoen, P. Athamanolap, A. P. O'Mullane, S.
46 Vongpunswad, Y. Poovorawan, S. Y. Lee and B. Lertanantawong, Rapid electrochemical
47 detection of coronavirus SARS-CoV-2, *Nat. Commun.*, 2021, **12**, 802.
- 48 164. A. Kaushik, A. Yndart, S. Kumar, R. D. Jayant, A. Vashist, A. N. Brown, C.-Z. Li and M. Nair, A
49 sensitive electrochemical immunosensor for label-free detection of Zika-virus protein, *Sci. Rep.*,
50 2018, **8**, 9700.
- 51 165. M. Z. M. Nasir, J. A. Jackman, N.-J. Cho, A. Ambrosi and M. Pumera, Detection of amphipathic
52 viral peptide on screen-printed electrodes by liposome rupture impact voltammetry, *Anal. Chem.*,
53 2017, **89**, 11753-11757.
- 54
55
56
57
58
59
60

- 1
2
3 166. D. J. Shirale, M. A. Bangar, M. Park, M. V. Yates, W. Chen, N. V. Myung and A. Mulchandani,
4 Label-free chemiresistive immunosensors for viruses, *Environ. Sci. Technol.*, 2010, **44**, 9030-9035.
5 167. N. Chartuprayoon, Y. Rheem, J. C. K. Ng, J. Nam, W. Chen and N. V. Myung, Polypyrrole
6 nanoribbon based chemiresistive immunosensors for viral plant pathogen detection, *Anal. Methods*,
7 2013, **5**, 3497-3502.
8 168. J. Vlasak and R. Ionescu, Fragmentation of monoclonal antibodies, *MAbs*, 2011, **3**, 253-263.
9 169. D. Wasik, A. Mulchandani and M. V. Yates, A heparin-functionalized carbon nanotube-based
10 affinity biosensor for dengue virus, *Biosens. Bioelectron.*, 2017, **91**, 811-816.
11 170. N. Varghese, U. Mogera, A. Govindaraj, A. Das, P. K. Maiti, A. K. Sood and C. Rao, Binding of
12 DNA nucleobases and nucleosides with graphene, *ChemPhysChem*, 2009, **10**, 206-210.
13 171. Y. Fu, V. Romay, Y. Liu, B. Ibarlucea, L. Baraban, V. Khavrus, S. Oswald, A. Bachmatiuk, I.
14 Ibrahim and M. Rümmele, Chemiresistive biosensors based on carbon nanotubes for label-free
15 detection of DNA sequences derived from avian influenza virus H5N1, *Sens. Actuators B: Chem.*,
16 2017, **249**, 691-699.
17 172. A. Bhasin, A. F. Ogata, J. S. Briggs, P. Y. Tam, M. X. Tan, G. A. Weiss and R. M. Penner, The
18 Virus Bioresistor: Wiring Virus Particles for the Direct, Label-Free Detection of Target Proteins,
19 *Nano Lett.*, 2018, **18**, 3623-3629.
20 173. K. I. Chen, B. R. Li and Y. T. Chen, Silicon nanowire field-effect transistor-based biosensors for
21 biomedical diagnosis and cellular recording investigation, *Nano Today*, 2011, **6**, 131-154.
22 174. M. O. Noor and U. J. Krull, Silicon nanowires as field-effect transducers for biosensor development:
23 A review, *Anal. Chim. Acta*, 2014, **825**, 1-25.
24 175. V. Schroeder, S. Savagatrup, M. He, S. B. Ling and T. M. Swager, Carbon Nanotube Chemical
25 Sensors, *Chem. Rev.*, 2019, **119**, 599-663.
26 176. J. S. Li, Y. L. Zhang, S. To, L. D. You and Y. Sun, Effect of Nanowire Number, Diameter, and
27 Doping Density on Nano-FET Biosensor Sensitivity, *ACS Nano*, 2011, **5**, 6661-6668.
28 177. W. Zhou, X. Dai and C. M. Lieber, Advances in nanowire bioelectronics, *Rep. Prog. Phys.*, 2016,
29 **80**, 016701.
30 178. X. Jin, H. Zhang, Y. T. Li, M. M. Xiao, Z. L. Zhang, D. W. Pang, G. Wong, Z. Y. Zhang and G. J.
31 Zhang, A field effect transistor modified with reduced graphene oxide for immunodetection of
32 Ebola virus, *Microchim. Acta*, 2019, **186**, 223.
33 179. G. Seo, G. Lee, M. J. Kim, S.-H. Baek, M. Choi, K. B. Ku, C.-S. Lee, S. Jun, D. Park and H. G.
34 Kim, Rapid Detection of COVID-19 Causative Virus (SARS-CoV-2) in Human Nasopharyngeal
35 Swab Specimens Using Field-Effect Transistor-Based Biosensor, *ACS Nano*, 2020, **14**, 5135-5142.
36 180. P. Fathi-Hafshejani, N. Azam, L. Wang, M. A. Kuroda, M. C. Hamilton, S. Hasim and M.
37 Mahjouri-Samani, Two-dimensional-material-based field-effect transistor biosensor for detecting
38 COVID-19 virus (SARS-CoV-2), *ACS Nano*, 2021, **15**, 11461-11469.
39 181. Y. T. Chen, R. Ren, H. H. Pu, X. R. Guo, J. B. Chang, G. H. Zhou, S. Mao, M. Kron and J. H.
40 Chen, Field-Effect Transistor Biosensor for Rapid Detection of Ebola Antigen, *Sci. Rep.*, 2017, **7**,
41 10974.
42 182. F. X. Shen, M. M. Tan, Z. X. Wang, M. S. Yao, Z. Q. Xu, Y. Wu, J. D. Wang, X. F. Guo and T.
43 Zhu, Integrating Silicon Nanowire Field Effect Transistor, Microfluidics and Air Sampling
44 Techniques For Real-Time Monitoring Biological Aerosols, *Environ. Sci. Technol.*, 2011, **45**,
45 7473-7480.
46 183. A. Maity, X. Sui, B. Jin, H. Pu, K. J. Bottum, X. Huang, J. Chang, G. Zhou, G. Lu and J. Chen,
47 Resonance-Frequency Modulation for Rapid, Point-of-Care Ebola-Glycoprotein Diagnosis with a
48 Graphene-Based Field-Effect Biotransistor, *Anal. Chem.*, 2018, **90**, 14230-14238.
49 184. M. Uhm, J. M. Lee, J. Lee, J. H. Lee, S. Choi, B. G. Park, D. M. Kim, S. J. Choi, H. S. Mo, Y. J.
50 Jeong and D. H. Kim, Ultrasensitive Electrical Detection of Hemagglutinin for Point-of-Care
51 Detection of Influenza Virus Based on a CMP-NANA Probe and Top-Down Processed Silicon
52 Nanowire Field-Effect Transistors, *Sensors*, 2019, **19**, 4502.
53
54
55
56
57
58
59
60

- 1
2
3 185. S. Park, H. Kim, K. Woo, J.-M. Kim, H.-J. Jo, Y. Jeong and K. H. Lee, SARS-CoV-2 Variant
4 Screening Using a Virus-Receptor-Based Electrical Biosensor, *Nano Lett.*, 2021, **22**, 50-57.
- 5 186. T. L. Tran, T. T. Nguyen, T. T. H. Tran, Q. T. Tran and A. T. Mai, Detection of influenza A virus
6 using carbon nanotubes field effect transistor based DNA sensor, *Phys. E: Low-Dimens. Syst.*
7 *Nanostructures*, 2017, **93**, 83-86.
- 8 187. J. Gao, C. Wang, C. Wang, Y. Chu, S. Wang, M. Y. Sun, H. Ji, Y. Gao, Y. Wang and Y. Han, Poly-
9 l-Lysine-Modified Graphene Field-Effect Transistor Biosensors for Ultrasensitive Breast Cancer
10 miRNAs and SARS-CoV-2 RNA Detection, *Anal. Chem.*, 2022, **94**, 1626-1636.
- 11 188. M. Shariati, The field effect transistor DNA biosensor based on ITO nanowires in label-free
12 hepatitis B virus detecting compatible with CMOS technology, *Biosens. Bioelectron.*, 2018, **105**,
13 58-64.
- 14 189. C. R. Tamanaha, S. P. Mulvaney, J. C. Rife and L. J. Whitman, Magnetic labeling, detection, and
15 system integration, *Biosens. Bioelectron.*, 2008, **24**, 1-13.
- 16 190. B. Srinivasan, Y. Li, Y. Jing, Y. Xu, X. Yao, C. Xing and J. P. Wang, A detection system based on
17 giant magnetoresistive sensors and high - moment magnetic nanoparticles demonstrates zeptomole
18 sensitivity: Potential for personalized medicine, *Angew. Chem. Int. Ed.*, 2009, **48**, 2764-2767.
- 19 191. D. Su, K. Wu, R. Saha, C. Peng and J.-P. Wang, Advances in Magnetoresistive Biosensors,
20 *Micromachines*, 2020, **11**, 34.
- 21 192. H. Yang, L. Chen, C. Lei, J. Zhang, D. Li, Z.-M. Zhou, C.-C. Bao, H.-Y. Hu, X. Chen and F. Cui,
22 Giant magnetoimpedance-based microchannel system for quick and parallel genotyping of human
23 papilloma virus type 16/18, *Appl. Phys. Lett.*, 2010, **97**, 043702.
- 24 193. X. Zhi, M. Deng, H. Yang, G. Gao, K. Wang, H. Fu, Y. Zhang, D. Chen and D. Cui, A novel HBV
25 genotypes detecting system combined with microfluidic chip, loop-mediated isothermal
26 amplification and GMR sensors, *Biosens. Bioelectron.*, 2014, **54**, 372-377.
- 27 194. V. D. Krishna, K. Wu, A. M. Perez and J.-P. Wang, Giant magnetoresistance-based biosensor for
28 detection of influenza A virus, *Front. Microbiol.*, 2016, **7**, 400.
- 29 195. K. Wu, T. Klein, V. D. Krishna, D. Su, A. M. Perez and J.-P. Wang, Portable GMR handheld
30 platform for the detection of influenza A virus, *ACS Sens.*, 2017, **2**, 1594-1601.
- 31 196. D. Su, K. Wu, V. Krishna, T. Klein, J. Liu, Y. Feng, A. M. Perez, M. C. Cheeran and J.-P. Wang,
32 Detection of influenza a virus in swine nasal swab samples with a wash-free magnetic bioassay and
33 a handheld giant magnetoresistance sensing system, *Front. Microbiol.*, 2019, **10**, 1077.
- 34 197. L. H. Reddy, J. L. Arias, J. Nicolas and P. Couvreur, Magnetic nanoparticles: design and
35 characterization, toxicity and biocompatibility, pharmaceutical and biomedical applications, *Chem.*
36 *Rev.*, 2012, **112**, 5818-5878.
- 37 198. I. Koh, R. Hong, R. Weissleder and L. Josephson, Nanoparticle– target interactions parallel
38 antibody– protein interactions, *Anal. Chem.*, 2009, **81**, 3618-3622.
- 39 199. J. M. Perez, F. J. Simeone, Y. Saeki, L. Josephson and R. Weissleder, Viral-induced self-assembly
40 of magnetic nanoparticles allows the detection of viral particles in biological media, *JACS*, 2003,
41 **125**, 10192-10193.
- 42 200. Y. P. Chen, Y. L. Xianyu, Y. Wang, X. Q. Zhang, R. T. Cha, J. S. Sun and X. Y. Jiang, One-Step
43 Detection of Pathogens and Viruses: Combining Magnetic Relaxation Switching and Magnetic
44 Separation, *ACS Nano*, 2015, **9**, 3184-3191.
- 45 201. C. J. Heneghan, E. A. Spencer, J. Brassey, A. Plüddemann, I. J. Onakpoya, D. H. Evans, J. M.
46 Conly and T. Jefferson, SARS-CoV-2 and the role of airborne transmission: a systematic review,
47 *F1000Research*, 2021, **10**, 232.
- 48 202. T. Yang and T. V. Duncan, Challenges and potential solutions for nanosensors intended for use
49 with foods, *Nat. Nanotechnol.*, 2021, **16**, 251-265.
- 50 203. G. La Rosa, P. Mancini, G. B. Ferraro, C. Veneri, M. Iaconelli, L. Bonadonna, L. Lucentini and E.
51 Suffredini, SARS-CoV-2 has been circulating in northern Italy since December 2019: Evidence
52 from environmental monitoring, *Sci. Total Environ.*, 2021, **750**, 141711.
- 53
54
55
56
57
58
59
60

- 1
2
3 204. I. D. Amoah, N. P. Mthethwa, L. Pillay, N. Deepnarain, K. Pillay, O. O. Awolusi, S. Kumari and
4 F. Bux, RT-LAMP: a cheaper, simpler and faster alternative for the detection of SARS-CoV-2 in
5 wastewater, *Food Environ. Virol.*, 2021, **13**, 447-456.
- 6 205. G. Sriram, M. P. Bhat, P. Patil, U. T. Uthappa, H.-Y. Jung, T. Altalhi, T. Kumeria, T. M.
7 Aminabhavi, R. K. Pai and M. D. Kurkuri, based microfluidic analytical devices for colorimetric
8 detection of toxic ions: A review, *TrAC, Trends Anal. Chem.*, 2017, **93**, 212-227.
- 9 206. A. L. Ferreira, L. F. de Lima, M. D. T. Torres, W. R. de Araujo and C. de la Fuente-Nunez, Low-
10 cost optodiagnostic for minute-time scale detection of SARS-CoV-2, *ACS Nano*, 2021, **15**, 17453-
11 17462.
- 12 207. K. Wu, R. Saha, D. Su, V. D. Krishna, J. Liu, M. C.-J. Cheeran and J.-P. Wang, Magnetic-
13 nanosensor-based virus and pathogen detection strategies before and during COVID-19, *ACS Appl.*
14 *Nano Mater.*, 2020, **3**, 9560-9580.
15
16
17
18
19
20
21
22
23
24
25
26
27
28
29
30
31
32
33
34
35
36
37
38
39
40
41
42
43
44
45
46
47
48
49
50
51
52
53
54
55
56
57
58
59
60